A micromechanical-statistical model based on hypersingular boundary integral equations for analyzing a pair of parallel interfaces weakened by antiplane micro-cracks*

X. Wang, W. T. Ang and H. Fan
School of Mechanical and Aerospace Engineering
Nanyang Technological University
Singapore 639798

Abstract

The estimation of the effective stiffness coefficients of a pair of microscopically damaged interfaces in a trimaterial under antiplane deformations is considered here. The trimaterial is made of a thin elastic layer sandwiched between two elastic half-spaces. The parallel planar interfaces are modeled as containing periodic arrays of randomly generated micro-cracks. The micromechanical-statistical model of the interfaces is formulated and numerically solved in terms of hypersingular boundary integral equations in which the displacement jumps across the micro-cracks are unknown functions. The numerical results obtained from the model demonstrate that the effective stiffness coefficients are influenced by the elastic moduli of the trimaterial, the thickness of the elastic layer and the densities of the micro-cracks.

Keywords: Micromechanics, microscopically damaged interface, effective stiffness, trimaterial, thin film, hypersingular boundary integral equations.

* Preprint of article in Computers & Structures 157 (2015) 178-188

1 Introduction

Multilayered structures play an increasingly important role in many engineering applications. Bonded layers of materials may be created by chemical or physical deposition processes (Knoll and Advincula [13]). During such processes, residual stresses may be induced by mismatches in the elastic or thermal properties of the different materials, giving rise to the formation of micro-cracks on the interface between two dissimilar materials (Zhang *et al.* [18]). Microscopic gaps may also exist on the interface because of the micro-roughness of surfaces. Thus, in general, the different layers in a multilayered structure are imperfectly bonded.

At the macro-level, an interface weakened by micro-defects may be modeled as a spring-like imperfect interface characterized by a stiffness tensor. In the macroscopic model, the displacement field is discontinuous across the spring-like interface and the tractions on the interface are linearly related to the displacement jumps over the interface (Benveniste and Miloh [4] and Jones and Whittier [11]).

Many researchers have studied boundary value problems involving the macro spring-like interface (see, for example, Ang [2], Fan and Wang [9] and Hashin [10]). There are, however, relatively few studies on the micromechanical estimation of the effective stiffness of the imperfect interface. Fan and Sze [8] presented a finite element based three-phase model for estimating the electric conduction coefficient of a micro-cracked interface between two dielectric half-spaces. The three-phase model takes into consideration only the density of the interfacial micro-cracks. To model the interface more realistically, Wang *et al.* [16] proposed a micromechanical-statistical approach in which the sizes and positions of the micro-cracks are randomly generated.

In [16], a selected number of micro-cracks of varying sizes are randomly

generated and positioned to form a finite interval of the microscopically damaged interface between two elastic half-spaces. The interval containing the micro-cracks is periodically reproduced on the remaining parts of the interface. The micromechanical-statistical model in [16] is formulated and solved in terms of hypersingular integral equations. In such a hypersingular integral formulation, the unknown functions are the displacement jumps over micro-cracks on the interface (Ang [3]). Thus, no post processing is needed to compute the interface displacement jumps which are required in estimating the effective stiffness of the interface. In [16], the micro-crack length is assumed to follow a normal distribution. For a more realistic distribution of the micro-crack sizes, Wang *et al.* [17] employed a chi-square (χ^2) distribution of a low degree of freedom to generate the micro-crack length.

The estimation of the effective stiffness coefficients of a pair of microscopically damaged interfaces in a trimaterial under antiplane deformations is considered in the current paper. The trimaterial is made of a thin elastic layer sandwiched between two elastic half-spaces. The micromechanical-statistical approach in [16] and [17] is used to model the two parallel planar interfaces. The resulting boundary value problem is formulated in terms of hypersingular boundary integral equations. Once the hypersingular boundary equations are solved, the effective stiffness coefficients of the interfaces may be readily computed. The effects of the elastic moduli of the trimaterial, the thickness of the elastic layer and the densities of the micro-cracks on the effective stiffness coefficients of the two interfaces are investigated.

2 A micromechanical problem of a pair of micro-cracked interfaces

With reference to a Cartesian coordinate system $Ox_1x_2x_3$, a thin elastic layer occupies the region $0 < x_2 < h$ and is sandwiched between two elastic half-spaces in the regions $x_2 < 0$ and $x_2 > h$. The interfaces $x_2 = 0$ and $x_2 = h$ between the layer and the half-spaces are microscopically damaged, containing interfacial micro-cracks. The micro-cracks have geometries independent of the x_3 coordinate. For convenience, the micro-cracked interfaces $x_2 = 0$ and $x_2 = h$ are denoted by I and II respectively.

The materials in the layer and half-spaces are anisotropic, having possibly dissimilar elastic properties. The trimaterial is assumed to undergo an antiplane elastostatic deformation along the x_3 direction. The x_1 and x_2 components of the elastic displacement are zero and the x_3 component, denoted by u_3, is a function of x_1 and x_2 only. According to Hooke's Law, the antiplane stresses σ_{3j} $(j = 1, 2)$ are related to the spatial derivatives of u_3 by

$$\sigma_{3j} = \lambda_{ij}(x_2)\frac{\partial u_3}{\partial x_i}, \tag{1}$$

where $\lambda_{ij}(x_2)$ are elastic moduli of the anisotropic materials given by

$$\lambda_{ij}(x_2) = \begin{cases} \lambda_{ij}^{(1)} & \text{for } x_2 > h, \\ \lambda_{ij}^{(2)} & \text{for } 0 < x_2 < h, \\ \lambda_{ij}^{(3)} & \text{for } x_2 < 0, \end{cases} \tag{2}$$

with $\lambda_{ij}^{(p)}$ being constants such that $\lambda_{ij}^{(p)} = \lambda_{ji}^{(p)}$ and $\lambda_{11}^{(p)}\lambda_{22}^{(p)} - (\lambda_{12}^{(p)})^2 > 0$. The usual Einsteinian convention of summing over a repeated index is assumed here for only Latin subscripts from 1 to 2.

From (1) and the equilibrium equations of elastostatics, the antiplane displacement u_3 satisfies the elliptic partial differential equation

$$\frac{\partial}{\partial x_j}(\lambda_{ij}(x_2)\frac{\partial u_3}{\partial x_i}) = 0. \tag{3}$$

If the displacement u_3 and stress σ_{3j} along a macroscopic portion of the microscopically damaged interface I or interface II is homogenized using

$$\begin{aligned}
\widehat{u}_3(\widehat{x}_1, 0^{\pm}) &= \frac{1}{2\ell}\int_{\widehat{x}_1-\ell}^{\widehat{x}_1+\ell} u_3(x_1, 0^{\pm})dx_1, \\
\widehat{u}_3(\widehat{x}_1, h^{\pm}) &= \frac{1}{2\ell}\int_{\widehat{x}_1-\ell}^{\widehat{x}_1+\ell} u_3(x_1, h^{\pm})dx_1, \\
\widehat{\sigma}_{3j}(\widehat{x}_1, 0^{\pm}) &= \frac{1}{2\ell}\int_{\widehat{x}_1-\ell}^{\widehat{x}_1+\ell} \sigma_{3j}(x_1, 0^{\pm})dx_1, \\
\widehat{\sigma}_{3j}(\widehat{x}_1, h^{\pm}) &= \frac{1}{2\ell}\int_{\widehat{x}_1-\ell}^{\widehat{x}_1+\ell} \sigma_{3j}(x_1, h^{\pm})dx_1, \qquad (4)
\end{aligned}$$

where $\widehat{x}_1$ and ℓ denote the midpoint and length of the macroscopic portion respectively, then the boundary conditions for the macro-level spring-like model for the interfaces are given by (see Wang *et al.* [16] and Hashin [10])

$$\begin{aligned}
\widehat{k}_{\mathrm{I}}\Delta\widehat{u}_{3\mathrm{I}}(\widehat{x}_1) &= \widehat{\sigma}_{32}(\widehat{x}_1, 0^+) = \widehat{\sigma}_{32}(\widehat{x}_1, 0^-), \\
\widehat{k}_{\mathrm{II}}\Delta\widehat{u}_{3\mathrm{II}}(\widehat{x}_1) &= \widehat{\sigma}_{32}(\widehat{x}_1, h^+) = \widehat{\sigma}_{32}(\widehat{x}_1, h^-), \qquad (5)
\end{aligned}$$

where $\Delta\widehat{u}_{3\mathrm{I}}(\widehat{x}_1) = \widehat{u}_3(x_1, 0^+) - \widehat{u}_3(x_1, 0^-)$ and $\Delta\widehat{u}_{3\mathrm{II}}(\widehat{x}_1) = \widehat{u}_3(x_1, h^+) - \widehat{u}_3(x_1, h^-)$ are the displacement jumps across interfaces I and II respectively and $\widehat{k}_{\mathrm{I}}$ and $\widehat{k}_{\mathrm{II}}$ denote the effective stiffness of interfaces I and II respectively. The two interfaces are assumed to be homogeneous at the macro level, hence the effective stiffness coefficients $\widehat{k}_{\mathrm{I}}$ and $\widehat{k}_{\mathrm{II}}$ are constant.

Note that the antiplane stress $\widehat{\sigma}_{32}$ in (5) is the antiplane traction on the micro-cracks. This is because the micro-cracks lie on the horizontal planes $x_2 = 0$ and $x_2 = h$.

At the microscopic level, the two interfaces are modeled as containing periodical arrays of interfacial micro-cracks. For a simplified model, each of the interfaces contains M arbitrarily positioned micro-cracks of possibly different lengths lying on a period interval of the interface of length L. On

the part of interface I where $0 < x_1 < L$, the tips of a typical m-th micro-crack are given by $(a_{\rm I}^{(m)}, 0)$ and $(b_{\rm I}^{(m)}, 0)$, where $a_{\rm I}^{(m)}$ and $b_{\rm I}^{(m)}$ are constants such that $0 < a_{\rm I}^{(1)} < b_{\rm I}^{(1)} < a_{\rm I}^{(2)} < b_{\rm I}^{(2)} < \cdots < a_{\rm I}^{(M)} < b_{\rm I}^{(M)} < L$. On the remaining parts of interface I, the interfacial micro-cracks lie at where $a_{\rm I}^{(m)} + nL < x_1 < b_{\rm I}^{(m)} + nL$, for $m = 1, 2, \cdots, M$ and $n = \pm 1, \pm 2, \cdots$. The part of interface II where $L_0 < x_1 < L_0 + L$ contains M micro-cracks with tips $(a_{\rm II}^{(m)}, 0)$ and $(b_{\rm II}^{(m)}, 0)$ (for $m = 1, 2, \cdots, M$), where L_0 is a given positive number such that $0 \leq L_0 < L$ and $a_{\rm II}^{(m)}$ and $b_{\rm II}^{(m)}$ are such that $L_0 < a_{\rm II}^{(1)} < b_{\rm II}^{(1)} < a_{\rm II}^{(2)} < b_{\rm II}^{(2)} < \cdots < a_{\rm II}^{(M)} < b_{\rm II}^{(M)} < L_0 + L$. The micro-cracks on interface II outside where $L_0 < x_1 < L_0 + L$ lie in the regions $a_{\rm II}^{(m)} + nL < x_1 < b_{\rm II}^{(m)} + nL$, $x_2 = 0$, for $m = 1, 2, \cdots, M$ and $n = \pm 1, \pm 2, \cdots$. Figure 1 gives a sketch of the geometry of the problem for $M = 3$. The uncracked parts of the interfaces are perfectly bonded.

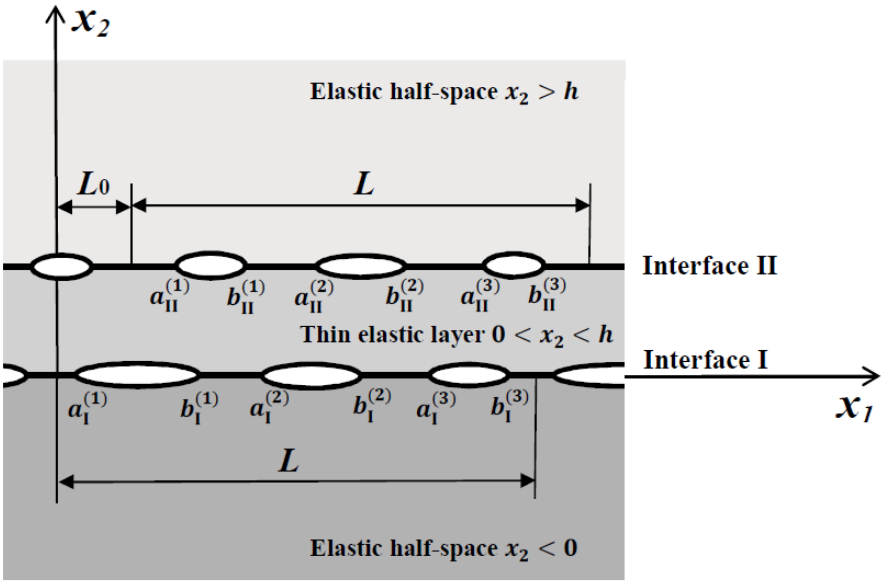

Figure 1. A sketch of the geometry of the problem for $M = 3$.

The damage ratios of interfaces I and II are respectively defined by

$$\rho_{\rm I} = \frac{1}{L}\sum_{m=1}^{M}(b_{\rm I}^{(m)} - a_{\rm I}^{(m)}) \text{ and } \rho_{\rm II} = \frac{1}{L}\sum_{m=1}^{M}(b_{\rm II}^{(m)} - a_{\rm II}^{(m)}). \tag{6}$$

From (6), because of the assumption that the two interfaces have the same number of micro-cracks, the damage ratios can be shown to be related to the average lengths of the micro-cracks on the interfaces by $\rho_{\rm I}/\rho_{\rm II} = \widehat{a}_{\rm I}/\widehat{a}_{\rm II}$, where $\widehat{a}_{\rm I}$ and $\widehat{a}_{\rm II}$ are the average lengths of the micro-cracks on interfaces I and II respectively.

A micromechanical problem of interest is to estimate the effective stiffness coefficients $\widehat{k}_{\rm I}$ and $\widehat{k}_{\rm II}$ of the pair of micro-cracked interfaces by taking into consideration some details of the micro-cracks.

3 Micromechanical-statistical model

3.1 Statistical approach

The micromechanical-statistical approach described in [16] and [17] is used here to estimate the stiffness coefficients $\widehat{k}_{\rm I}$ and $\widehat{k}_{\rm II}$ of the pair of micro-cracked interfaces. A pair of micro-cracked interfaces is randomly formed as follows. The lengths of the M micro-cracks (within a period length of each of the interfaces) are randomly generated to follow a chi-square distribution of degree of freedom k, which is denoted by $\chi^2(k)$. The micro-crack length distribution on interface I may be different from that on interface II. The distance L_0 in Figure 1 is also randomly determined within the range $0 \leq L_0 < L$. The micro-cracks are positioned randomly on over the period intervals $0 < x_1 < L$ and $L_0 < x_1 < L_0 + L$ on interfaces I and II respectively.

For fixed values of the elastic constants $\lambda_{ij}^{(p)}$ $(p = 1, 2, 3)$ in (2), the non-dimensionalized thickness $h/\widehat{a}_{\rm I}$ of the layer and the damage ratios $\rho_{\rm I}$ and $\rho_{\rm II}$ in

(6), N pairs of micro-cracked interfaces are generated randomly as described above for estimating the effective stiffness of interfaces I and II. (Note that all the interfaces contain the same number of micro-cracks per period interval of the interface.) If the non-dimensionalized effective stiffness coefficients $\widehat{a}_{\rm I}\widehat{k}_{\rm I}/\lambda_{22}^{(2)}$ and $\widehat{a}_{\rm II}\widehat{k}_{\rm II}/\lambda_{22}^{(2)}$ of the n-th pair of interfaces are respectively given by $Y_{\rm I}^{(n)}$ and $Y_{\rm II}^{(n)}$ $(n = 1, 2, \cdots, N)$, then the mean value $\mu_{\rm I}$ of $\widehat{a}_{\rm I}\widehat{k}_{\rm I}/\lambda_{22}^{(2)}$ and the standard deviation $s_{\rm I}$ of $\widehat{a}_{\rm I}\widehat{k}_{\rm I}/\lambda_{22}^{(2)}$ from the mean are given by

$$\mu_{\rm I} = \frac{1}{N}\sum_{n=1}^{N} Y_{\rm I}^{(n)} \text{ and } s_{\rm I} = \sqrt{\frac{1}{N-1}\sum_{n=1}^{N}(Y_{\rm I}^{(n)} - \mu_{\rm I})^2}, \tag{7}$$

and the mean value $\mu_{\rm II}$ of $\widehat{a}_{\rm II}\widehat{k}_{\rm II}/\lambda_{22}^{(2)}$ and the corresponding standard deviation $s_{\rm II}$ by

$$\mu_{\rm II} = \frac{1}{N}\sum_{n=1}^{N} Y_{\rm II}^{(n)} \text{ and } s_{\rm II} = \sqrt{\frac{1}{N-1}\sum_{n=1}^{N}(Y_{\rm II}^{(n)} - \mu_{\rm II})^2}. \tag{8}$$

3.2 Boundary value problem

The boundary value problem to solve for the micromechanical-statistical model in order to estimate the stiffness coefficients of the interfaces is stated below.

The trimaterial is subject to an external antiplane shear stress load at infinity. The micro-cracks along interfaces I and II are assumed to be traction-free. The displacement u_3 and the stress σ_{32} are continuous across the uncracked parts of the interfaces. Mathematically, the conditions on interfaces

I and II are given by

$$\begin{aligned}
&\sigma_{32}(x_1,0^{\pm})=0 \text{ for } (x_1,0)\in D_{\rm I},\\
&\sigma_{32}(x_1,h^{\pm})=0 \text{ for } (x_1,h)\ \in D_{\rm II},\\
&\left.\begin{array}{rcl}\Delta u_{3\rm I}(x_1) &=& 0\\ \sigma_{32}(x_1,0^{+}) &=& \sigma_{32}(x_1,0^{-})\end{array}\right\} \text{ for } (x_1,0)\ \in P_{\rm I},\\
&\left.\begin{array}{rcl}\Delta u_{3\rm II}(x_1) &=& 0\\ \sigma_{32}(x_1,h^{+}) &=& \sigma_{32}(x_1,h^{-})\end{array}\right\} \text{ for } (x_1,h)\ \in P_{\rm II},
\end{aligned}\tag{9}$$

where $\Delta u_{3\rm I}(x_1)=u_3(x_1,0^+)-u_3(x_1,0^-)$, $\Delta u_{3\rm II}(x_1)=u_3(x_1,h^+)-u_3(x_1,h^-)$, $D_{\rm I}$ and $D_{\rm II}$ denote the micro-cracked parts of interfaces I and II respectively and $P_{\rm I}$ and $P_{\rm II}$ denote the perfectly bonded parts of interfaces I and II respectively.

If the displacement u_3 and the stress σ_{32} are written as

$$\begin{aligned}
u_3 &= u_3^{(\rm ext)}+u_3^{(\rm imp)},\\
\sigma_{32} &= \sigma_{32}^{(\rm ext)}+\sigma_{32}^{(\rm imp)},
\end{aligned}\tag{10}$$

where $u_3^{(\rm ext)}$ and $\sigma_{32}^{(\rm ext)}$ are respectively the displacement and the stress fields in the trimaterial for the corresponding case where the interfaces I and II do not contain any micro-crack, then (9) may be rewritten as

$$\begin{aligned}
&\sigma_{32}^{(\rm imp)}(x_1,0^{\pm})=-\sigma_{32}^{(\rm ext)}(x_1,0^{\pm}) \text{ for } (x_1,0)\in D_{\rm I},\\
&\sigma_{32}^{(\rm imp)}(x_1,h^{\pm})=-\sigma_{32}^{(\rm ext)}(x_1,h^{\pm}) \text{ for } (x_1,h)\ \in D_{\rm II},\\
&\left.\begin{array}{rcl}\Delta u_{3\rm I}^{(\rm imp)}(x_1) &=& 0\\ \sigma_{32}^{(\rm imp)}(x_1,0^{+}) &=& \sigma_{32}^{(\rm imp)}(x_1,0^{-})\end{array}\right\} \text{ for } (x_1,0)\ \in P_{\rm I},\\
&\left.\begin{array}{rcl}\Delta u_{3\rm II}^{(\rm imp)}(x_1) &=& 0\\ \sigma_{32}^{(\rm imp)}(x_1,h^{+}) &=& \sigma_{32}^{(\rm imp)}(x_1,h^{-})\end{array}\right\} \text{ for } (x_1,h)\ \in P_{\rm II},
\end{aligned}\tag{11}$$

where $\Delta u_{3\rm I}^{(\rm imp)}(x_1)$ and $\Delta u_{3\rm II}^{(\rm imp)}(x_1)$ are respectively defined by $\Delta u_{3\rm I}^{(\rm imp)}(x_1)=u_3^{(\rm imp)}(x_1,0^+)-u_3^{(\rm imp)}(x_1,0^-)$ and $\Delta u_{3\rm II}^{(\rm imp)}(x_1)=u_3^{(\rm imp)}(x_1,h^+)-u_3^{(\rm imp)}(x_1,h^-)$.

Note that $u_3^{(\mathrm{imp})}$ and $\sigma_{32}^{(\mathrm{imp})}$ may be regarded as respectively the displacement and the stress induced by the micro-cracks. The load acting on the trimaterial at infinity is assumed to be such that $u_3^{(\mathrm{ext})}$, $\sigma_{32}^{(\mathrm{ext})}$, $u_3^{(\mathrm{imp})}$ and $\sigma_{32}^{(\mathrm{imp})}$ are periodic functions of x_1 with period L on any plane $x_2 = c$ (constant).

With $u_3^{(\mathrm{ext})}$ and $\sigma_{32}^{(\mathrm{ext})}$ assumed given, the boundary value problem of interest here is to solve the partial differential equation (3) together with (2) subject to the interfacial conditions in (11) and the far field condition given by $\sigma_{32}^{(\mathrm{imp})} \to 0$ as $|x_2| \to \infty$. In Subsection 3.3 below, it (the boundary value problem) is formulated in terms of hypersingular boundary integral equations with the displacement jumps $\Delta u_{3\mathrm{I}}^{(\mathrm{imp})}(x_1)$ and $\Delta u_{3\mathrm{II}}^{(\mathrm{imp})}(x_1)$ across the micro-cracks as unknown functions to be determined.

Once the displacement jumps $\Delta u_{3\mathrm{I}}^{(\mathrm{imp})}(x_1)$ and $\Delta u_{3\mathrm{II}}^{(\mathrm{imp})}(x_1)$ across the micro-cracks are determined, the effective stiffness $\widehat{k}_{\mathrm{I}}$ and $\widehat{k}_{\mathrm{II}}$ may be estimated by using

$$\begin{aligned}
\widehat{k}_{\mathrm{I}} \sum_{k=1}^{M} \int_{a_{\mathrm{I}}^{(k)}}^{b_{\mathrm{I}}^{(k)}} \Delta u_{3\mathrm{I}}^{(\mathrm{imp})}(x_1) dx_1 &= \int_0^L \sigma_{32}^{(\mathrm{ext})}(x_1, 0) dx_1, \\
\widehat{k}_{\mathrm{II}} \sum_{k=1}^{M} \int_{a_{\mathrm{II}}^{(k)}}^{b_{\mathrm{II}}^{(k)}} \Delta u_{3\mathrm{II}}^{(\mathrm{imp})}(x_1) dx_1 &= \int_{L_0}^{L_0+L} \sigma_{32}^{(\mathrm{ext})}(x_1, h) dx_1. \qquad (12)
\end{aligned}$$

3.3 Hypersingular boundary integral equations

To formulate the boundary value problem in Subsection 3.2 above in terms of hypersingular boundary integral equations, the trimaterial in Figure 1 is divided up into two separate subdomains defined by $x_2 > h/2$ and $x_2 < h/2$. The boundary integral equations for antiplane elasticity (in Clements [7]) are then used together with the Green's function for a perfect interface between two half-spaces (in Berger and Tewary [5]) to derive hypersingular boundary integral equations separately for each of the subdomains.

From the boundary integral equations for the lower subdomain $x_2 < h/2$, the hypersingular boundary integral equations for the stress $\sigma_{32}^{(\mathrm{imp})}$ on the artificial boundary $x_2 = h^-/2$ and interface I (where $x_2 = 0^+$) are respectively given by

$$\begin{aligned}
&\frac{1}{2}\sigma_{32}^{(\mathrm{imp})}(\xi_1, h^-/2) \\
= \; & -\frac{1}{2\pi}\oint_0^L u_3^{(\mathrm{imp})}(x_1, h^-/2)[\frac{1}{(x_1-\xi_1)^2} + \Theta(x_1,\xi_1)]dx_1 \\
& + \frac{1}{2\pi}\frac{\beta^{(2)}-\beta^{(3)}}{\beta^{(2)}+\beta^{(3)}}\int_0^L u_3^{(\mathrm{imp})}(x_1, h^-/2)\,\mathrm{Re}\{\Omega(x_1,\xi_1,(\tau^{(2)}-\overline{\tau}^{(2)})h^-/2)\}dx_1 \\
& - \frac{\beta^{(2)}-\beta^{(3)}}{2\pi(\beta^{(2)}+\beta^{(3)})}\int_0^L \sigma_{32}^{(\mathrm{imp})}(x_1, h^-/2)\,\mathrm{Re}\{\Gamma(x_1,\xi_1,(\tau^{(2)}-\overline{\tau}^{(2)})h^-/2)\}dx_1 \\
& + \frac{\beta^{(3)}}{\pi(\beta^{(2)}+\beta^{(3)})}\sum_{k=1}^{M}\int_{a_{\mathrm{I}}^{(k)}}^{b_{\mathrm{I}}^{(k)}} \Delta u_{3\mathrm{I}}^{(\mathrm{imp})}(x_1)\,\mathrm{Re}\{\Omega(x_1,\xi_1,-\tau^{(2)}h^-/2)\}dx_1 \\
& \text{for } 0 < \xi_1 < L, \qquad (13)
\end{aligned}$$

and

$$\begin{aligned}
& \int_0^L u_3^{(\mathrm{imp})}(x_1, h^-/2)\,\mathrm{Re}\{\Omega(x_1,\xi_1,\tau^{(2)}h^-/2)\}dx_1 \\
& - \int_0^L \sigma_{32}^{(\mathrm{imp})}(x_1, h^-/2)\,\mathrm{Re}\{\Gamma(x_1,\xi_1,\tau^{(2)}h^-/2)\}dx_1 \\
& - \sum_{k=1}^{M}\oint_{a_{\mathrm{I}}^{(k)}}^{b_{\mathrm{I}}^{(k)}} \Delta u_{3\mathrm{I}}^{(\mathrm{imp})}(x_1)[\frac{1}{(x_1-\xi_1)^2} + \Theta(x_1,\xi_1)]dx_1 \\
= \; & \frac{\pi}{\beta^{(3)}}(\beta^{(2)}+\beta^{(3)})\sigma_{32}^{(\mathrm{ext})}(\xi_1, 0) \\
& \text{for } a_{\mathrm{I}}^{(n)} < \xi_1 < b_{\mathrm{I}}^{(n)} \text{ for } n = 1, 2, ..., M. \qquad (14)
\end{aligned}$$

where $\oint$ denotes that the integral is to be interpreted in the Hadamard finite-part sense, $\beta^{(p)} = \sqrt{\lambda_{11}^{(p)}\lambda_{22}^{(p)} - [\lambda_{12}^{(p)}]^2}$, $\tau^{(p)} = (-\lambda_{12}^{(p)} + i\beta^{(p)})/\lambda_{22}^{(p)}$, $i = \sqrt{-1}$,

$\Theta(x_1,\xi_1)$, $\Omega(x_1,\xi_1,z)$ and $\Gamma(x_1,\xi_1,z)$ are defined by

$$\begin{aligned}
\Theta(x_1,\xi_1) &= \frac{1}{L^2}\Psi_1(\frac{L+x_1-\xi_1}{L})+\frac{1}{L^2}\Psi_1(\frac{L+\xi_1-x_1}{L}),\\
\Omega(x_1,\xi_1,z) &= \frac{1}{(x_1-\xi_1+z)^2}+\frac{1}{L^2}\Psi_1(\frac{L+x_1-\xi_1+z}{L})\\
&\quad+\frac{1}{L^2}\Psi_1(\frac{L-x_1+\xi_1-z}{L}),\\
\Gamma(x_1,\xi_1,z) &= \frac{i}{x_1-\xi_1+z}-\frac{i}{L}\Psi(\frac{L+x_1-\xi_1+z}{L})\\
&\quad+\frac{i}{L}\Psi(\frac{L-x_1+\xi_1-z}{L}),
\end{aligned}\tag{15}$$

with $\Psi(z)$ and $\Psi_1(z)$ being the digamma and trigamma functions respectively (See Abramowitz and Stegun [1]). Note that (14) is derived from the interfacial conditions on $D_{\rm I}$ and $P_{\rm I}$ in (11).

From the boundary integral equations for the upper subdomain $x_2 > h/2$, the hypersingular integral equations for the stress $\sigma_{32}^{(\rm imp)}$ on the artificial boundary $x_2 = h^+/2$ and interface II (where $x_2 = h^-$) are given by

$$\begin{aligned}
&\frac{1}{2}\sigma_{32}^{(\rm imp)}(\xi_1,h^+/2)\\
=\;& \frac{1}{2\pi}\!\!=\!\!\!\!\!\!\int_{L_0}^{L_0+L} u_3^{(\rm imp)}(x_1,h^+/2)[\frac{1}{(x_1-\xi_1)^2}+\Theta(x_1,\xi_1)]dx_1\\
&-\frac{\beta^{(2)}-\beta^{(1)}}{2\pi(\beta^{(2)}+\beta^{(1)})}\int_{L_0}^{L_0+L} u_3^{(\rm imp)}(x_1,h^+/2)\\
&\times \mathrm{Re}\{\Omega(x_1,\xi_1,-(\tau^{(2)}-\overline{\tau}^{(2)})h^+/2)\}dx_1\\
&+\frac{\beta^{(2)}-\beta^{(1)}}{2\pi(\beta^{(2)}+\beta^{(1)})}\int_{L_0}^{L_0+L} \sigma_{32}^{(\rm imp)}(x_1,h^+/2)\\
&\times \mathrm{Re}\{\Gamma(x_1,\xi_1,-(\tau^{(2)}-\overline{\tau}^{(2)})h^+/2)\}dx_1\\
&+\frac{\beta^{(1)}}{\pi(\beta^{(2)}+\beta^{(1)})}\sum_{k=1}^{M}\int_{a_{\rm II}^{(k)}}^{b_{\rm II}^{(k)}} \Delta u_{3\rm II}^{(\rm imp)}(x_1)\,\mathrm{Re}\{\Omega(x_1,\xi_1,\tau^{(2)}h^+/2)\}dx_1\\
&\text{for } L_0<\xi_1<L_0+L,
\end{aligned}\tag{16}$$

and

$$\begin{aligned}
&\int_{L_0}^{L_0+L} u_3^{(\mathrm{imp})}(x_1, h^+/2)\,\mathrm{Re}\{\Omega(x_1,\xi_1,-\tau^{(2)}h^+/2)\}dx_1 \\
&-\int_{L_0}^{L_0+L} \sigma_{32}^{(\mathrm{imp})}(x_1, h^+/2)\,\mathrm{Re}\{\Gamma(x_1,\xi_1,-\tau^{(2)}h^+/2)\}dx_1 \\
&+\sum_{k=1}^{M} \neq\!\!\!\int_{a_{\mathrm{II}}^{(k)}}^{b_{\mathrm{II}}^{(k)}} \Delta u_{3\mathrm{II}}^{(\mathrm{imp})}(x_1)[\frac{1}{(x_1-\xi_1)^2}+\Theta(x_1,\xi_1)]dx_1 \\
= \;& -\frac{\pi}{\beta^{(1)}}(\beta^{(2)}+\beta^{(1)})\sigma_{32}^{(\mathrm{ext})}(\xi_1,h) \\
&\text{for } a_{\mathrm{II}}^{(n)} < \xi_1 < b_{\mathrm{II}}^{(n)} \text{ for } n = 1,2,...,M. \qquad (17)
\end{aligned}$$

In (13), (14), (16) and (17), the unknown functions are the displacement jumps $\Delta u_{3\mathrm{I}}^{(\mathrm{imp})}(x_1)$ and $\Delta u_{3\mathrm{II}}^{(\mathrm{imp})}(x_1)$ across the micro-cracks on interfaces I and II respectively, the displacements $u_3^{(\mathrm{imp})}(x_1, h^+/2)$ and $u_3^{(\mathrm{imp})}(x_1, h^-/2)$ and the stresses $\sigma_{32}^{(\mathrm{imp})}(x_1, h^+/2)$ and $\sigma_{32}^{(\mathrm{imp})}(x_1, h^-/2)$. There are six unknown functions but only four equations. To complete the formulation, continuity conditions are imposed on the artificially created boundary $x_2 = h/2$ as follows:

$$\left.\begin{array}{l} u_3^{(\mathrm{imp})}(x_1, h^+/2) = u_3^{(\mathrm{imp})}(x_1, h^-/2) \\ \sigma_{32}^{(\mathrm{imp})}(x_1, h^+/2) = \sigma_{32}^{(\mathrm{imp})}(x_1, h^-/2) \end{array}\right\} \text{ for } -\infty < x_1 < \infty. \qquad (18)$$

Note that $\Delta u_{3\mathrm{I}}^{(\mathrm{imp})}(x_1)$, $\Delta u_{3\mathrm{II}}^{(\mathrm{imp})}(x_1)$, $u_3^{(\mathrm{imp})}(x_1, h^{\pm}/2)$ and $\sigma_{32}^{(\mathrm{imp})}(x_1, h^{\pm}/2)$ are all periodic functions of x_1 with period L.

Once $\Delta u_{3\mathrm{I}}^{(\mathrm{imp})}(x_1)$ and $\Delta u_{3\mathrm{II}}^{(\mathrm{imp})}(x_1)$ are obtained by solving the hypersingular boundary integral equations (13), (14), (16) and (17) together with (18), the effective stiffness $\widehat{k}_{\mathrm{I}}$ and $\widehat{k}_{\mathrm{II}}$ for the interface I and interface II respectively may be estimated by using (12).

3.4 Numerical procedure

The numerical procedure for solving the boundary hypersingular integral equations in (13), (14), (16) and (17) together with (18) is outlined here.

The unknowns $u_3^{(\mathrm{imp})}(x_1, h^-/2)$ and $\sigma_{32}^{(\mathrm{imp})}(x_1, h^-/2)$ in (13) are defined for $0 \le x_1 \le L$, while the unknowns $u_3^{(\mathrm{imp})}(x_1, h^+/2)$ and $\sigma_{32}^{(\mathrm{imp})}(x_1, h^+/2)$ in (16) are defined for $L_0 \le x_1 \le L_0 + L$. For the numerical treatment of (13) and (16), the interval $0 \le x_1 \le L_0$ is divided into N_0 equal length elements given by $x^{(p)} \le x_1 \le x^{(p+1)}$ for $p = 1, 2, \cdots, N_0$, the interval $L_0 \le x_1 \le L$ into N_1 equal length elements given by $x^{(N_0+p)} \le x_1 \le x^{(N_0+p+1)}$ for $p = 1, 2, \cdots, N_1$, and the interval $L \le x_1 \le L + L_0$ into N_0 equal length elements given by $x^{(N_0+N_1+p)} \le x_1 \le x^{(N_0+p+1)}$ for $p = 1, 2, \cdots, N_0$. Thus, the interval $0 \le x_1 \le L + L_0$ is discretized into $2N_0 + N_1$ elements. For convenience, the element defined by $x^{(m)} \le x_1 \le x^{(m+1)}$ is denoted by $E^{(m)}$ ($m = 1, 2, \cdots, 2N_0 + N_1$).

From (18), the functions $u_3^{(\mathrm{imp})}(x_1, h^\pm/2)$ and $\sigma_{32}^{(\mathrm{imp})}(x_1, h^\pm/2)$ may be approximated over the first $N_0 + N_1$ elements (in the interval $0 \le x_1 \le L$) by

$$\left.\begin{array}{l} u_3^{(\mathrm{imp})}(x_1, h^\pm/2) \simeq x_1\phi^{(m)} + \psi^{(m)} \\ \sigma_{32}^{(\mathrm{imp})}(x_1, h^\pm/2) \simeq x_1\vartheta^{(m)} + \eta^{(m)} \end{array}\right\} \text{ over } E^{(m)} \ (m = 1, 2, \cdots, N_0 + N_1), \tag{19}$$

where $\phi^{(m)}$, $\psi^{(m)}$, $\vartheta^{(m)}$ and $\eta^{(m)}$ are constants yet to be determined. Since $u_3^{(\mathrm{imp})}(x_1, h^\pm/2)$ and $\sigma_{32}^{(\mathrm{imp})}(x_1, h^\pm/2)$ are periodic functions of x_1 with period L, they may be approximated over the last N_0 elements (in $L \le x_1 \le L + L_0$) by using

$$\left.\begin{array}{l} u_3^{(\mathrm{imp})}(x_1, h^\pm/2) \simeq (x_1 - L)\phi^{(m)} + \psi^{(m)} \\ \sigma_{32}^{(\mathrm{imp})}(x_1, h^\pm/2) \simeq (x_1 - L)\vartheta^{(m)} + \eta^{(m)} \end{array}\right\} \text{ over } E^{(m)}$$
$$(m = N_0 + N_1 + 1, N_0 + N_1 + 2, \cdots, N_0 + N_1 + N_0), \tag{20}$$

Note that the approximations for the antiplane displacement and traction in (19) and (20) are the discontinuous linear elements described in París and Cañas [14]. Such approximations give more accurate results than the constant elements.

The number of unknown constants in (19) and (20) is $4(N_0 + N_1)$. The hypersingular boundary integral equations in (13) and (16) may be collocated over $0 < \xi_1 < L$ and $L_0 < \xi_1 < L_0 + L$ respectively to generate $4(N_0 + N_1)$ equations. For this purpose, two collocation points are chosen in the interior of each element. Specifically, on the element $E^{(m)}$, the two interior collocation points are given by

$$y_1^{(m)} = \frac{1}{4}x_1^{(m)} + \frac{3}{4}x_1^{(m+1)} \text{ and } y_2^{(m)} = \frac{3}{4}x_1^{(m)} + \frac{1}{4}x_1^{(m+1)} \quad (m = 1, 2, \cdots, N_0 + N_1). \tag{21}$$

Note that the elements involved in (13) are $E^{(1)}$, $E^{(2)}$, $\cdots$, $E^{(N_0+N_1-1)}$ and $E^{(N_0+N_1)}$ (the first N_0+N_1 elements), while those in (16) are $E^{(N_0+1)}$, $E^{(N_0+2)}$, $\cdots$, $E^{(2N_0+N_1-1)}$ and $E^{(2N_0+N_1)}$ (the last $N_0 + N_1$ elements).

As in Kaya and Erdogan [12], to incorporate the correct behaviors of the displacement jumps $\Delta u_{3\mathrm{I}}^{(\mathrm{imp})}(x_1)$ and $\Delta u_{3\mathrm{II}}^{(\mathrm{imp})}(x_1)$ across the micro-cracks on interfaces I and II respectively, we make the approximation

$$\begin{aligned} \Delta u_{3\mathrm{I}}^{(\mathrm{imp})}(x_1) &\simeq \sqrt{(x_1 - a_{\mathrm{I}}^{(k)})(b_{\mathrm{I}}^{(k)} - x_1)} \\ &\quad \times \sum_{m=1}^{N_{\mathrm{I}}^{(k)}} \alpha_{\mathrm{I}}^{(km)} U^{(m-1)}\left(\frac{2x_1 - b_{\mathrm{I}}^{(k)} - a_{\mathrm{I}}^{(k)}}{b_{\mathrm{I}}^{(k)} - a_{\mathrm{I}}^{(k)}}\right) \\ \text{for } a_{\mathrm{I}}^{(k)} &< x_1 < b_{\mathrm{I}}^{(k)} \ (k = 1, 2, ..., M), \end{aligned} \tag{22}$$

and

$$\begin{aligned}\Delta u_{3\mathrm{II}}^{(\mathrm{imp})}(x_1) &\simeq \sqrt{(x_1-a_{\mathrm{II}}^{(k)})(b_{\mathrm{II}}^{(k)}-x_1)} \\ &\quad \times \sum_{m=1}^{N_{\mathrm{II}}^{(k)}} \alpha_{\mathrm{II}}^{(km)} U^{(m-1)}\Big(\frac{2x_1-b_{\mathrm{II}}^{(k)}-a_{\mathrm{II}}^{(k)}}{b_{\mathrm{II}}^{(k)}-a_{\mathrm{II}}^{(k)}}\Big) \\ \text{for } a_{\mathrm{II}}^{(k)} &< x_1 < b_{\mathrm{II}}^{(k)} \ (k=1,2,...,M), \end{aligned} \tag{23}$$

where $\alpha_{\mathrm{I}}^{(km)}$ and $\alpha_{\mathrm{II}}^{(km)}$ are constants yet to be determined, $N_{\mathrm{I}}^{(k)}$ and $N_{\mathrm{II}}^{(k)}$ are positive integers and $U^{(m)}(x_1)$ is the m-th order Chebyshev polynomial of the second kind. Different approaches for approximating the displacement jumps across the cracks may be found in Ang [3]. The approximations in (22) and (23) give a very accurate and efficient numerical technique for analyzing cracks.

There are $(N_{\mathrm{I}}^{(1)}+N_{\mathrm{I}}^{(2)}+\cdots+N_{\mathrm{I}}^{(M)}+N_{\mathrm{II}}^{(1)}+N_{\mathrm{II}}^{(2)}+\cdots+N_{\mathrm{II}}^{(M)})$ unknown constants in (22) and (23). The hypersingular boundary equations in (14) and (17) may be collocated over $a_{\mathrm{I}}^{(n)} < \xi_1 < b_{\mathrm{I}}^{(n)}$ and $a_{\mathrm{II}}^{(n)} < \xi_1 < b_{\mathrm{II}}^{(n)}$ to generate $(N_{\mathrm{I}}^{(1)}+N_{\mathrm{I}}^{(2)}+\cdots+N_{\mathrm{I}}^{(M)}+N_{\mathrm{II}}^{(1)}+N_{\mathrm{II}}^{(2)}+\cdots+N_{\mathrm{II}}^{(M)})$ equations. Specifically, the collocation points over $a_{\mathrm{I}}^{(n)} < \xi_1 < b_{\mathrm{I}}^{(n)}$ are given by

$$\begin{aligned} z_{\mathrm{I}}^{(nm)} &= \frac{a_{\mathrm{I}}^{(n)}+b_{\mathrm{I}}^{(n)}}{2} + \frac{b_{\mathrm{I}}^{(n)}-a_{\mathrm{I}}^{(n)}}{2}\cos\Big(\frac{[2m-1]\pi}{2N_{\mathrm{I}}^{(n)}}\Big) \\ &\qquad \text{for } m=1,2,\cdots,N_{\mathrm{I}}^{(n)} \ (n=1,2,...,M), \end{aligned} \tag{24}$$

and those over $a_{\mathrm{II}}^{(n)} < \xi_1 < b_{\mathrm{II}}^{(n)}$ by

$$\begin{aligned} z_{\mathrm{II}}^{(nm)} &= \frac{a_{\mathrm{II}}^{(n)}+b_{\mathrm{II}}^{(n)}}{2} + \frac{b_{\mathrm{II}}^{(n)}-a_{\mathrm{II}}^{(n)}}{2}\cos\Big(\frac{[2m-1]\pi}{2N_{\mathrm{II}}^{(n)}}\Big) \\ &\qquad \text{for } m=1,2,\cdots,N_{\mathrm{II}}^{(n)} \ (n=1,2,...,M). \end{aligned} \tag{25}$$

If the approximations (19), (20), (22) and (23) are substituted into (13), (14), (16) and (17), the hypersingular boundary equations (13) and (16) are

collocated at $y_i^{(m)}$ $(i = 1, 2)$ (in (21)) for $m = 1, 2, \cdots, N_0 + N_1$ and $m = N_0+1, N_0+2, \cdots, 2N_0+N_1$ respectively and (14) and (17) at the collocation points defined in (24) and (25) respectively, a system of linear algebraic equations can be set up for determining all the yet to be determined constant coefficients in (19), (20), (22) and (23). The linear algebraic equations are solved without any difficulty by using the LU decomposition technique (Press *et al.* [15]). Once $\alpha_{\rm I}^{(km)}$ and $\alpha_{\rm II}^{(km)}$ are determined, (22) and (23) may be substituted into (12) to compute $\widehat{k}_{\rm I}$ and $\widehat{k}_{\rm II}$ approximately.

4 A numerical verification of the hypersingular boundary integral equations

A three-phase model based on the self-consistent scheme of Christensen and Lo [6] may be developed for estimating the effective stiffness of a micro-cracked interface. In such a model, the interface is made up of a simplified micro-structure and an effective region interacting with each other (see Fan and Sze [8] and Wang *et al.* [16]). The model is of limited applicability, as it takes into consideration only the density of the micro-cracks on the interface. However, as shown numerically in [16], it may provide a good approximation for an interface that contains a periodic array of evenly distributed micro-cracks of equal length.

Thus, for a numerical verification that the hypersingular boundary integral equations in (13), (14), (16) and (17) are correctly derived, one may compare the numerical solution of these equations for the special case of evenly distributed micro-cracks with the solution for a three-phase model of the pair of micro-cracked interfaces.

4.1 Crack tips of evenly distributed micro-cracks on the pair of interfaces

All the micro-cracks on interface I have the same length $2a_{\rm I}$. The distance L_0 in Figure 1 is taken to be zero. They are evenly distributed on the interface, so that the tips $(a_{\rm I}^{(m)}, 0)$ and $(b_{\rm I}^{(m)}, 0)$ of the m-th micro-crack in the portion of interface I where $0 < x_1 < L$, $x_2 = 0$ are given by

$$\left.\begin{array}{rcl} a_{\rm I}^{(1)} = \dfrac{L}{2M}(1-\rho_{\rm I}), & & b_{\rm I}^{(1)} = a_{\rm I}^{(1)} + 2a_{\rm I}, \\ a_{\rm I}^{(m)} & = & a_{\rm I}^{(m-1)} + \dfrac{L}{M} \\ b_{\rm I}^{(m)} & = & a_{\rm I}^{(m)} + 2a_{\rm I} \end{array}\right\} \text{ for } m = 2, 3, \cdots, M. \tag{26}$$

Similarly, the tips $(a_{\rm II}^{(m)}, h)$ and $(b_{\rm II}^{(m)}, h)$ of the M evenly distributed micro-cracks of equal length $2a_{\rm II}$, which lie in the portion of interface II where $0 < x_1 < L$, $x_2 = h$, are given by

$$\left.\begin{array}{rcl} a_{\rm II}^{(1)} = \dfrac{L}{2M}(1-\rho_{\rm II}), & & b_{\rm II}^{(1)} = a_{\rm II}^{(1)} + 2a_{\rm II}, \\ a_{\rm II}^{(m)} & = & a_{\rm II}^{(m-1)} + \dfrac{L}{M} \\ b_{\rm II}^{(m)} & = & a_{\rm II}^{(m)} + 2a_{\rm II} \end{array}\right\} \text{ for } m = 2, 3, \cdots, M. \tag{27}$$

4.2 A three-phase model for the pair of interfaces

A geometrical sketch of the three-phase model for interfaces I and II is shown in Figure 2. Each of the interfaces is made up of three components: micro-cracked, perfectly bonded and effective regions. In Figure 2, all the three components are clearly shown in the region $0 < x_1 < L$ on interfaces I and II. The geometries of the interfaces are periodic with period L. The length of the effective region on each of the interfaces is assumed to be very large compared to the lengths of the micro-crack and the perfectly bonded part on the interface. Note that $c_{\rm I}^{(1)} = c_{\rm I}^{(2)} - d_{\rm I}^{(1)}$ and $c_{\rm II}^{(1)} = c_{\rm II}^{(2)} - d_{\rm II}^{(1)}$.

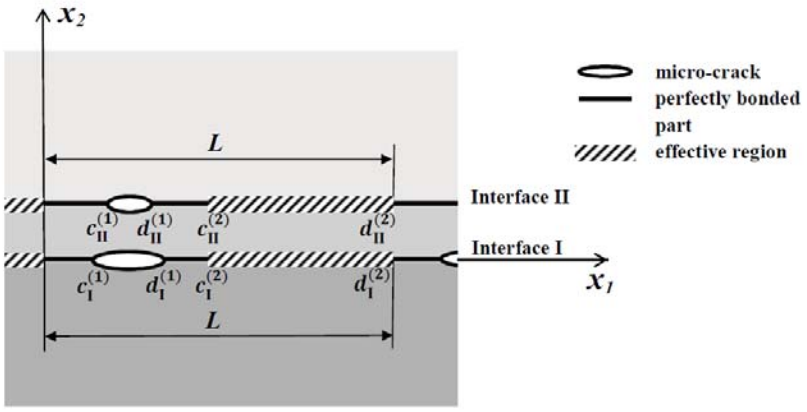

Figure 2. A geometrical sketch of the three-phase model for interfaces I and II.

For the three-phase model, the damage ratios for the interface I and interface II corresponding to (6) are respectively given by

$$\rho_{\rm I} = \frac{d_{\rm I}^{(1)} - c_{\rm I}^{(1)}}{c_{\rm I}^{(2)}} \quad \text{and} \quad \rho_{\rm II} = \frac{d_{\rm II}^{(1)} - c_{\rm II}^{(1)}}{c_{\rm II}^{(2)}}. \tag{28}$$

As in the micromechanical-statistical model, the displacement u_3 and the stress σ_{32} maybe written into the form in (10), where $u_3^{(\rm ext)}$ and $\sigma_{32}^{(\rm ext)}$ are respectively the displacement and the stress fields in the trimaterial for the corresponding case where the entire interfaces I and II are perfectly bonded, and $u_3^{(\rm imp)}$ and $\sigma_{32}^{(\rm imp)}$ are respectively the displacement and stress due to the interaction between the micro-cracks and the effective regions. As before, the internal stress fields $\sigma_{32}^{(\rm ext)}(x_1, 0)$ and $\sigma_{32}^{(\rm ext)}(x_1, h)$ are assumed known.

The interfacial conditions for the three-phase model are given by

$$\begin{aligned}
&\sigma_{32}^{(\mathrm{imp})}(x_1,0^{\pm}) = -\sigma_{32}^{(\mathrm{ext})}(x_1,0) \text{ for } (x_1,0) \in D_{\mathrm{I}},\\
&\sigma_{32}^{(\mathrm{imp})}(x_1,h^{\pm}) = -\sigma_{32}^{(\mathrm{ext})}(x_1,h) \text{ for } (x_1,h) \ \in D_{\mathrm{II}},\\
&\left.\begin{array}{rcl} \Delta u_{3\mathrm{I}}^{(\mathrm{imp})}(x_1) &=& 0\\ \sigma_{32}^{(\mathrm{imp})}(x_1,0^{+}) &=& \sigma_{32}^{(\mathrm{imp})}(x_1,0^{-}) \end{array}\right\} \text{ for } (x_1,0) \ \in P_{\mathrm{I}},\\
&\left.\begin{array}{rcl} \Delta u_{3\mathrm{II}}^{(\mathrm{imp})}(x_1) &=& 0\\ \sigma_{32}^{(\mathrm{imp})}(x_1,h^{+}) &=& \sigma_{32}^{(\mathrm{imp})}(x_1,h^{-}) \end{array}\right\} \text{ for } (x_1,h) \ \in P_{\mathrm{II}},\\
&\widehat{k}_{\mathrm{I}}\Delta u_{3\mathrm{I}}^{(\mathrm{imp})}(x_1) = \sigma_{32}^{(\mathrm{ext})}(x_1,0) + \sigma_{32}^{(\mathrm{imp})}(x_1,0^{\pm}) \text{ for } (x_1,0) \ \in E_{\mathrm{I}},\\
&\widehat{k}_{\mathrm{II}}\Delta u_{3\mathrm{II}}^{(\mathrm{imp})}(x_1) = \sigma_{32}^{(\mathrm{ext})}(x_1,h) \ + \sigma_{32}^{(\mathrm{imp})}(x_1,h^{\pm}) \text{ for } (x_1,h) \ \in E_{\mathrm{II}}, \qquad (29)
\end{aligned}$$

where D_{I} and D_{II} denote the micro-cracked parts of interfaces I and II respectively, P_{I} and P_{II} denote the perfectly bonded parts of interfaces I and II respectively and E_{I} and E_{II} denote the effective regions on interfaces I and II respectively.

The effective regions E_{I} and E_{II} behave according to the macro spring-like interface model in (5) but with unknown (yet to determined) effective stiffness $\widehat{k}_{\mathrm{I}}$ and $\widehat{k}_{\mathrm{II}}$. As $\widehat{k}_{\mathrm{I}}$ and $\widehat{k}_{\mathrm{II}}$ in (29) are unknown coefficients, two more equations are needed to complete the formulation for the three-phase model. They are given by

$$\begin{aligned}
\widehat{k}_{\mathrm{I}} \int_{c_{\mathrm{I}}^{(1)}}^{d_{\mathrm{I}}^{(1)}} \Delta u_{3\mathrm{I}}^{(\mathrm{imp})}(x_1)dx_1 &= \int_0^{c_{\mathrm{I}}^{(2)}} \sigma_{32}^{(\mathrm{ext})}(x_1,0)dx_1,\\
\widehat{k}_{\mathrm{II}} \int_{c_{\mathrm{II}}^{(1)}}^{d_{\mathrm{II}}^{(1)}} \Delta u_{3\mathrm{II}}^{(\mathrm{imp})}(x_1)dx_1 &= \int_0^{c_{\mathrm{II}}^{(2)}} \sigma_{32}^{(\mathrm{ext})}(x_1,h)dx_1. \qquad (30)
\end{aligned}$$

As in the analysis in Subsection 3.3, the trimaterial in Figure 2 is divided into the subdomains $x_2 < h/2$ and $x_2 > h/2$ to derive hypersingular boundary integral equations for the three-phase model.

From the boundary integral equations for the lower subdomain $x_2 < h/2$, the hypersingular integral equations for the stress $\sigma_{32}^{(\mathrm{imp})}$ on the artificial

boundary $x_2 = h^-/2$ and interface I (where $x_2 = 0^+$) are respectively given by

$$
\begin{aligned}
&\frac{1}{2}\sigma_{32}^{(\mathrm{imp})}(\xi_1, h^-/2) \\
= \; & -\frac{1}{2\pi}\Xint=_0^L u_3^{(\mathrm{imp})}(x_1, h^-/2)[\frac{1}{(x_1-\xi_1)^2} + \Theta(x_1,\xi_1)]dx_1 \\
& + \frac{1}{2\pi}\frac{\beta^{(2)}-\beta^{(3)}}{\beta^{(2)}+\beta^{(3)}}\int_0^L u_3^{(\mathrm{imp})}(x_1, h^-/2)\,\mathrm{Re}\{\Omega(x_1,\xi_1,(\tau^{(2)}-\overline{\tau}^{(2)})h^-/2)\}dx_1 \\
& - \frac{\beta^{(2)}-\beta^{(3)}}{2\pi(\beta^{(2)}+\beta^{(3)})}\int_0^L \sigma_{32}^{(\mathrm{imp})}(x_1, h^-/2)\,\mathrm{Re}\{\Gamma(x_1,\xi_1,(\tau^{(2)}-\overline{\tau}^{(2)})h^-/2)\}dx_1 \\
& + \frac{\beta^{(3)}}{\pi(\beta^{(2)}+\beta^{(3)})}\sum_{k=1}^{2}\int_{c_{\mathrm{I}}^{(k)}}^{d_{\mathrm{I}}^{(k)}} \Delta u_{3\mathrm{I}}^{(\mathrm{imp})}(x_1)\,\mathrm{Re}\{\Omega(x_1,\xi_1,-\tau^{(2)}h^-/2)\}dx_1 \\
& \text{for } 0<\xi_1<L. \qquad (31)
\end{aligned}
$$

and

$$
\begin{aligned}
& \int_0^L u_3^{(\mathrm{imp})}(x_1, h^-/2)\,\mathrm{Re}\{\Omega(x_1,\xi_1,\tau^{(2)}h^-/2)\}dx_1 \\
& - \int_0^L \sigma_{32}^{(\mathrm{imp})}(x_1, h^-/2)\,\mathrm{Re}\{\Gamma(x_1,\xi_1,\tau^{(2)}h^-/2)\}dx_1 \\
& - \Xint=_{c_{\mathrm{I}}^{(n)}}^{d_{\mathrm{I}}^{(n)}} \frac{\Delta u_{3\mathrm{I}}^{(\mathrm{imp})}(x_1)}{(x_1-\xi_1)^2}dx_1 \\
& - \sum_{\substack{k=1\\k\neq n}}^{2}\int_{c_{\mathrm{I}}^{(k)}}^{d_{\mathrm{I}}^{(k)}} \frac{\Delta u_{3\mathrm{I}}^{(\mathrm{imp})}(x_1)}{(x_1-\xi_1)^2}dx_1 \\
& - \sum_{k=1}^{2}\int_{c_{\mathrm{I}}^{(k)}}^{d_{\mathrm{I}}^{(k)}} \Delta u_{3\mathrm{I}}^{(\mathrm{imp})}(x_1)\Theta(x_1,\xi_1)dx_1 \\
= \; & \frac{\pi(\beta^{(2)}+\beta^{(3)})(\sigma_{32}^{(\mathrm{ext})}(\xi_1,0) - \delta^{(n2)}\widehat{k}_{\mathrm{I}}\Delta u_{3\mathrm{I}}^{(\mathrm{imp})}(\xi_1))}{\beta^{(3)}} \\
& \text{for } c_{\mathrm{I}}^{(n)} < \xi_1 < d_{\mathrm{I}}^{(n)} \text{ for } n=1,2. \qquad (32)
\end{aligned}
$$

where $\delta^{(n2)}$ is such that $\delta^{(12)} = 0$ and $\delta^{(22)} = 1$.

From the boundary integral equations for the upper subdomain $x_2 > h/2$, the hypersingular integral equations for the stress $\sigma_{32}^{(\mathrm{imp})}$ on the artificial boundary $x_2 = h^+/2$ and interface II (where $x_2 = h^-$) are

$$
\begin{aligned}
& \frac{1}{2}\sigma_{32}^{(\mathrm{imp})}(\xi_1, h^+/2) \\
= \; & \frac{1}{2\pi}\!\!\!\!\!\!\int_0^L u_3^{(\mathrm{imp})}(x_1, h^+/2)[\frac{1}{(x_1-\xi_1)^2} + \Theta(x_1,\xi_1)]dx_1 \\
& -\frac{\beta^{(2)}-\beta^{(1)}}{2\pi(\beta^{(2)}+\beta^{(1)})}\int_0^L u_3^{(\mathrm{imp})}(x_1, h^+/2) \\
& \times \mathrm{Re}\{\Omega(x_1,\xi_1,-(\tau^{(2)}-\overline{\tau}^{(2)})h^+/2)\}dx_1 \\
& +\frac{\beta^{(2)}-\beta^{(1)}}{2\pi(\beta^{(2)}+\beta^{(1)})}\int_0^L \sigma_{32}^{(\mathrm{imp})}(x_1, h^+/2) \\
& \times \mathrm{Re}\{\Gamma(x_1,\xi_1,-(\tau^{(2)}-\overline{\tau}^{(2)})h^+/2)\}dx_1 \\
& +\frac{\beta^{(1)}}{\pi(\beta^{(2)}+\beta^{(1)})}\sum_{k=1}^{2}\int_{c_{\mathrm{II}}^{(k)}}^{d_{\mathrm{II}}^{(k)}} \Delta u_{3\mathrm{II}}^{(\mathrm{imp})}(x_1)\,\mathrm{Re}\{\Omega(x_1,\xi_1,\tau^{(2)}h^+/2)\}dx_1 \\
& \text{for } 0<\xi_1<L, \qquad (33)
\end{aligned}
$$

and

$$
\begin{aligned}
&\int_0^L u_3^{(\mathrm{imp})}(x_1, h^+/2)\,\mathrm{Re}\{\Omega(x_1,\xi_1,-\tau^{(2)}h^-/2)\}dx_1 \\
&-\int_0^L \sigma_{32}^{(\mathrm{imp})}(x_1, h^+/2)\,\mathrm{Re}\{\Gamma(x_1,\xi_1,-\tau^{(2)}h^-/2)\}dx_1 \\
&+\!\!\!\!\!\!=\!\!\!\!\!\!\int_{c_{\mathrm{II}}^{(n)}}^{d_{\mathrm{II}}^{(n)}} \frac{\Delta u_{3\mathrm{II}}^{(\mathrm{imp})}(x_1)}{(x_1-\xi_1)^2}dx_1 \\
&+\sum_{\substack{k=1\\k\neq n}}^{2}\int_{c_{\mathrm{II}}^{(k)}}^{d_{\mathrm{II}}^{(k)}} \frac{\Delta u_{3\mathrm{II}}^{(\mathrm{imp})}(x_1)}{(x_1-\xi_1)^2}dx_1 \\
&+\sum_{k=1}^{2}\int_{c_{\mathrm{II}}^{(k)}}^{d_{\mathrm{II}}^{(k)}} \Delta u_{3\mathrm{II}}^{(\mathrm{imp})}(x_1)\Theta(x_1,\xi_1)dx_1 \\
=\;& \frac{\pi(\beta^{(2)}+\beta^{(1)})(-\sigma_{32}^{(\mathrm{ext})}(\xi_1,h)+\delta^{(n2)}\widehat{k}_{\mathrm{II}}\Delta u_{3\mathrm{II}}^{(\mathrm{imp})}(\xi_1))}{\beta^{(1)}} \\
&\text{for } c_{\mathrm{II}}^{(n)} < \xi_1 < d_{\mathrm{II}}^{(n)} \text{ for } n=1,2. \qquad (34)
\end{aligned}
$$

The hypersingular boundary integral equations (31), (32), (33) and (34) are to be solved numerically together with (30) for $\Delta u_{3\mathrm{I}}^{(\mathrm{imp})}(x_1)$, $\Delta u_{3\mathrm{II}}^{(\mathrm{imp})}(x_1)$, $u_3^{(\mathrm{imp})}(x_1, h^{\pm}/2)$, $\sigma_{32}^{(\mathrm{imp})}(x_1, h^{\pm}/2)$ and $\widehat{k}_{\mathrm{I}}$ and $\widehat{k}_{\mathrm{II}}$.

For the approximation of $u_3^{(\mathrm{imp})}(x_1, h^-/2)$ and $\sigma_{32}^{(\mathrm{imp})}(x_1, h^-/2)$, the interval $0 \le x_1 \le L$ is discretized into elements as described in Subsection 3.4 and (19) and (20) are still valid here. As in (22) and (23), the displacement jumps $\Delta u_{3\mathrm{I}}^{(\mathrm{imp})}(x_1)$ and $\Delta u_{3\mathrm{II}}^{(\mathrm{imp})}(x_1)$ over the micro-cracks $c_{\mathrm{I}}^{(1)} < x_1 < d_{\mathrm{I}}^{(1)}$, $x_2 = 0$ (interface I) and $c_{\mathrm{II}}^{(1)} < x_1 < d_{\mathrm{II}}^{(1)}$, $x_2 = h$ (interface II) are given by

$$
\begin{aligned}
\Delta u_{3\mathrm{I}}^{(\mathrm{imp})}(x_1) \;\simeq\; & \sqrt{(x_1-c_{\mathrm{I}}^{(1)})(d_{\mathrm{I}}^{(1)}-x_1)} \\
& \times \sum_{m=1}^{N_{\mathrm{I}}} \alpha_{\mathrm{I}}^{(m)} U^{(m-1)}\Big(\frac{2x_1-d_{\mathrm{I}}^{(1)}-c_{\mathrm{I}}^{(1)}}{d_{\mathrm{I}}^{(1)}-c_{\mathrm{I}}^{(1)}}\Big) \\
& \text{for } c_{\mathrm{I}}^{(1)} < x_1 < d_{\mathrm{I}}^{(1)}, \qquad (35)
\end{aligned}
$$

and

$$\Delta u_{3\mathrm{II}}^{(\mathrm{imp})}(x_1) \simeq \sqrt{(x_1 - c_{\mathrm{II}}^{(1)})(d_{\mathrm{II}}^{(1)} - x_1)} \times \sum_{m=1}^{N_{\mathrm{II}}} \alpha_{\mathrm{II}}^{(m)} U^{(m-1)}\left(\frac{2x_1 - d_{\mathrm{II}}^{(1)} - c_{\mathrm{II}}^{(1)}}{d_{\mathrm{II}}^{(1)} - c_{\mathrm{II}}^{(1)}}\right) \quad \text{for } c_{\mathrm{II}}^{(1)} < x_1 < d_{\mathrm{II}}^{(1)}. \tag{36}$$

For approximating the unknown function $\Delta u_{3\mathrm{I}}^{(\mathrm{imp})}(x_1)$ over the effective region on interface I, the interval $c_{\mathrm{I}}^{(2)} < x_1 < d_{\mathrm{I}}^{(2)}$ is discretized into N_2 equal length elements given by $E_{\mathrm{I}}^{(1)}$, $E_{\mathrm{I}}^{(2)}$, $\cdots$, $E_{\mathrm{I}}^{(N_2-1)}$ and $E_{\mathrm{I}}^{(N_2)}$. Similarly, for $\Delta u_{3\mathrm{II}}^{(\mathrm{imp})}(x_1)$ over the effective region on interface II, the interval $c_{\mathrm{II}}^{(2)} < x_1 < d_{\mathrm{II}}^{(2)}$ is discretized into N_3 equal length elements given by $E_{\mathrm{II}}^{(1)}$, $E_{\mathrm{II}}^{(2)}$, $\cdots$, $E_{\mathrm{II}}^{(N_3-1)}$ and $E_{\mathrm{II}}^{(N_3)}$. The displacement jumps $\Delta u_{3\mathrm{I}}^{(\mathrm{imp})}(x_1)$ and $\Delta u_{3\mathrm{II}}^{(\mathrm{imp})}(x_1)$ over the effective regions on interfaces I and II respectively are approximated using

$$\Delta u_{3\mathrm{I}}^{(\mathrm{imp})}(x_1) \simeq x_1 \omega_{\mathrm{I}}^{(m)} + \gamma_{\mathrm{I}}^{(m)} \text{ over } E_{\mathrm{I}}^{(m)} \ (m = 1, 2, \cdots, N_2), \tag{37}$$

and

$$\Delta u_{3\mathrm{II}}^{(\mathrm{imp})}(x_1) \simeq x_1 \omega_{\mathrm{II}}^{(m)} + \gamma_{\mathrm{II}}^{(m)} \text{ over } E_{\mathrm{II}}^{(m)} \ (m = 1, 2, \cdots, N_3), \tag{38}$$

where $\omega_{\mathrm{I}}^{(p)}$, $\gamma_{\mathrm{I}}^{(p)}$, $\omega_{\mathrm{II}}^{(p)}$ and $\gamma_{\mathrm{II}}^{(p)}$ are constants yet to be determined.

The hypersingular boundary integral equations (31), (32), (33) and (34) may be discretized and collocated as explained in Subsection 3.4 to obtain a system of linear algebraic equations with the unknown effective stiffness coefficients $\widehat{k}_{\mathrm{I}}$ and $\widehat{k}_{\mathrm{II}}$ and coefficients in the approximations of the unknown functions in the integral equations. However, the discretization of the two equations in (30) give rise to a pair of quadratic equations in the unknown constants. The algebraic equations may be solved numerically by using an iterative procedure as described in Wang *et al.* [16].

4.3 Numerical comparison of the effective stiffness coefficients

The values of the effective stiffness coefficients $\widehat{k}_{\rm I}$ and $\widehat{k}_{\rm II}$ computed by solving numerically the hypersingular boundary integral equations in Subsection 3.3 for the evenly distributed micro-cracks described in Subsection 4.1 are compared here with those calculated using the corresponding three-phase model in Subsection 4.2. The two sets of values are expected to be close to each other. This may be used as a numerical check that the equations in Subsections 3.3 and 3.4 and the three-phase model are correctly derived.

For the calculations here, the trimaterial is taken to be isotropic with elastic moduli $\lambda_{ij}^{(n)} = \delta_{ij} G^{(n)}$ $(n = 1, 2, 3)$, where δ_{ij} is the kronecker-delta, $G^{(1)}$ and $G^{(3)}$ are the constant shear modulus of the half-spaces $x_2 > h$ and $x_2 < 0$ respectively and $G^{(2)}$ is the constant shear modulus of the thin elastic layer. The internal loads $\sigma_{32}^{(\rm ext)}(x_1, 0)$ and $\sigma_{32}^{(\rm ext)}(x_1, h)$ in (12) and (30) are taken to be S_0, where S_0 is a given constant. In (26) and (27), M is chosen to be 10. The lengths of the micro-cracks on interfaces I and II in Figure 1 are given by the positive real numbers $2a_{\rm I}$ and $2a_{\rm II}$ respectively. In the three-phase model as sketched in Figure 2, the coordinates $c_{\rm I}^{(1)}$, $d_{\rm I}^{(1)}$, $c_{\rm II}^{(1)}$ and $d_{\rm II}^{(1)}$ are such that $d_{\rm I}^{(1)} - c_{\rm I}^{(1)} = 2a_{\rm I}$ and $d_{\rm II}^{(1)} - c_{\rm II}^{(1)} = 2a_{\rm II}$. For convenience, we take $c_{\rm I}^{(2)} = c_{\rm II}^{(2)}$.

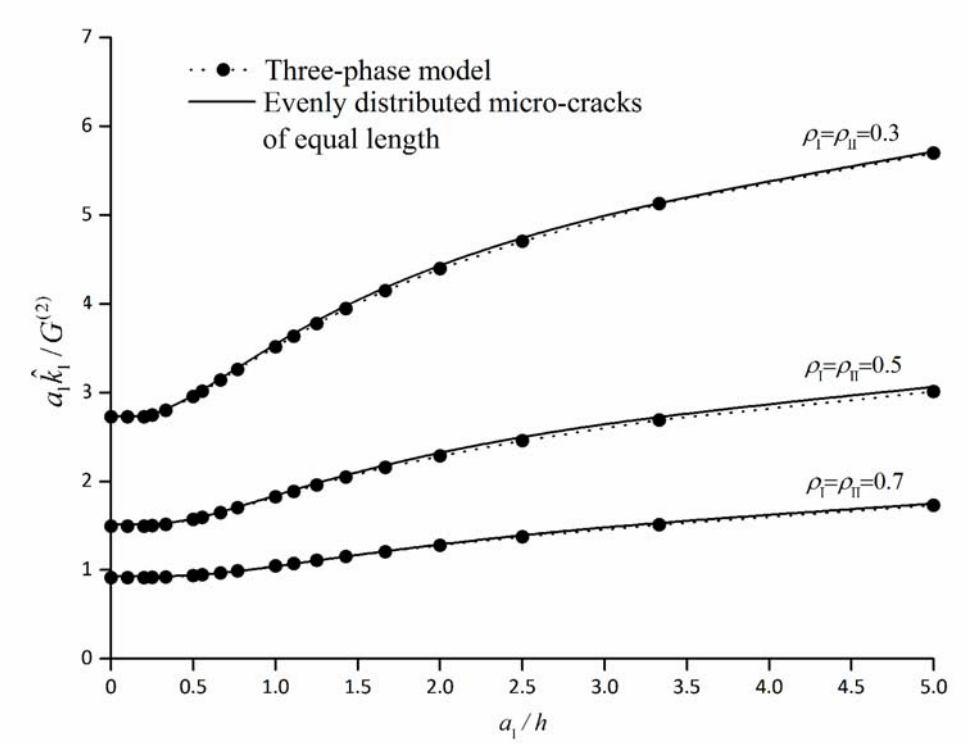

Figure 3. Plots of $a_{\rm I}\widehat{k}_{\rm I}/G^{(2)}$ against $a_{\rm I}/h$ for $G^{(1)}/G^{(2)} = G^{(3)}/G^{(2)} = 2$ and $\rho_{\rm I} = \rho_{\rm II} = 0.3$, 0.5 and 0.7.

For $G^{(1)}/G^{(2)} = G^{(3)}/G^{(2)} = 2$, we plot and compare the two sets of the non-dimensionalized effective stiffness coefficient $a_{\rm I}\widehat{k}_{\rm I}/G^{(2)}$ against $a_{\rm I}/h$ for $\rho_{\rm I} = \rho_{\rm II} = 0.3$, 0.5 and 0.7 in Figure 3. Note that here $a_{\rm I}\widehat{k}_{\rm I}/G^{(2)} = a_{\rm II}\widehat{k}_{\rm II}/G^{(2)}$. The plots obtained by the numerical procedure in Subsection 3.4 are close to the ones from the corresponding three-phase model in Subsection 4.2. For a fixed $\rho_{\rm I}$ in Figure 3, the percentage difference between the values of $a_{\rm I}\widehat{k}_{\rm I}/G^{(2)}$ for the two models for a selected $a_{\rm I}/h$ is less than 1.6%. This indicates that the hypersingular boundary integral equations in Subsection 3.3 are properly derived.

For the special case where $a_{\rm I}/h \to 0^+$, Fan and Sze [8] had proposed a

finite element based three-phase model for estimating the effective stiffness of the interface. For a very small value of $a_{\rm I}/h$ like $a_{\rm I}/h = 0.001$, we have checked that the values of the non-dimensionalized effective stiffness for selected values of $\rho_{\rm I}$ and $\rho_{\rm II}$ in Figure 3 are in agreement to within 5.4% with the finite element calculated values in [8]. The finite element calculation in [8] involves over 10000 linear algebraic equations. In comparison, for small values of $a_{\rm I}/h$, our calculation requires less than a hundred linear algebraic equations.

5 Micromechanical-statistical simulations

The micromechanical-statistical model is used here for estimating the effective stiffness coefficients for the interfaces I and II. As explained in Subsection 3.1, a pair of interfaces are formed by randomly generating interfaces I and II and randomly choosing the distance L_0 within the range $0 \leq L_0 < L$. For both interfaces I and II, the M micro-cracks over a period interval of each interface have randomly generated sizes. For each interface, the micro-crack length follows a chosen χ^2 distribution. The micro-cracks are randomly positioned over a period length L of each interface. For selected values of $\rho_{\rm I}$, $\rho_{\rm II}$, $\widehat{a}_{\rm I}/h$, $G^{(1)}/G^{(2)}$ and $G^{(3)}/G^{(2)}$, N pairs of randomly generated interfaces form a sample to generate the statistical data for the effective stiffness of interfaces I and II. For each pair of the interfaces, $\widehat{a}_{\rm I}\widehat{k}_{\rm I}/G^{(2)}$ and $\widehat{a}_{\rm II}\widehat{k}_{\rm II}/G^{(2)}$ are calculated as explained in Subsection 3.4. The non-dimensionalized effective stiffness coefficients are given by the means of $\widehat{a}_{\rm I}\widehat{k}_{\rm I}/G^{(2)}$ and $\widehat{a}_{\rm II}\widehat{k}_{\rm II}/G^{(2)}$ calculated from the N pairs of randomly generated interfaces. As in Subsection 4.3, both the internal loads $\sigma_{32}^{(\rm ext)}(x_1, 0)$ and $\sigma_{32}^{(\rm ext)}(x_1, h)$ are taken to be the positive constant S_0.

5.1 Number of micro-cracks required for homogenizing the effective stiffness coefficients

The number of micro-cracks required on a period interval of each interface for homogenizing the effective stiffness of the interface is examined here. For fixed values of $\rho_{\rm I}$, $\rho_{\rm II}$, $\widehat{a}_{\rm I}/h$, $G^{(1)}/G^{(2)}$ and $G^{(3)}/G^{(2)}$, 50 pairs of interfaces are randomly generated. The lengths of micro-cracks on interface I and interface II follow a $\chi^2(k_1)$ and a $\chi^2(k_2)$ distribution respectively, where k_1 and k_2 are positive integers. If each interface requires M_0 micro-cracks per period interval for homogenizing the effective stiffness of the interface, the mean values of $\widehat{a}_{\rm I}\widehat{k}_{\rm I}/G^{(2)}$ and $\widehat{a}_{\rm II}\widehat{k}_{\rm II}/G^{(2)}$ from the 50 pairs of interfaces should not vary much for $M \geq M_0$.

For $\rho_{\rm I} = 0.7$, $\rho_{\rm II} = 0.5$, $\widehat{a}_{\rm I}/h = 1$, $G^{(1)}/G^{(2)} = 0.5$ and $G^{(3)}/G^{(2)} = 2$, Figure 4 gives the scatter plots of the data for $\widehat{a}_{\rm I}\widehat{k}_{\rm I}/G^{(2)}$ and $\widehat{a}_{\rm II}\widehat{k}_{\rm II}/G^{(2)}$ against various values of M, for the case where the micro-crack length for each of the two micro-cracked interfaces follows the $\chi^2(5)$ distribution. The means of $\widehat{a}_{\rm I}\widehat{k}_{\rm I}/G^{(2)}$ and $\widehat{a}_{\rm II}\widehat{k}_{\rm II}/G^{(2)}$ are also included in Figure 4 for the different values of M. It is obvious that both the means for $\widehat{a}_{\rm I}\widehat{k}_{\rm I}/G^{(2)}$ and $\widehat{a}_{\rm II}\widehat{k}_{\rm II}/G^{(2)}$ decrease significantly as M increases from 10 to 40 and do not change very much when M exceeds 40. Moreover, the scatter range of the data for the non-dimensionalized effective stiffness of the 50 pairs of interfaces does not change significantly as M increases from 40 to 60 and is much narrower than the scattering range of the data for M between 10 and 40. For both interfaces I and II, it appears that 40 micro-cracks per period interval of each interface may be sufficient for homogenizing the non-dimensionalized effective stiffness of the interface.

Further investigations carried out by using various other values for $\rho_{\rm I}$, $\rho_{\rm II}$, $\widehat{a}_{\rm I}/h$, $G^{(1)}/G^{(2)}$, $G^{(3)}/G^{(2)}$, k_1 and k_2 also suggest that 40 micro-cracks

per period interval of each interface are needed to homogenize the non-dimensionalized effective stiffness.

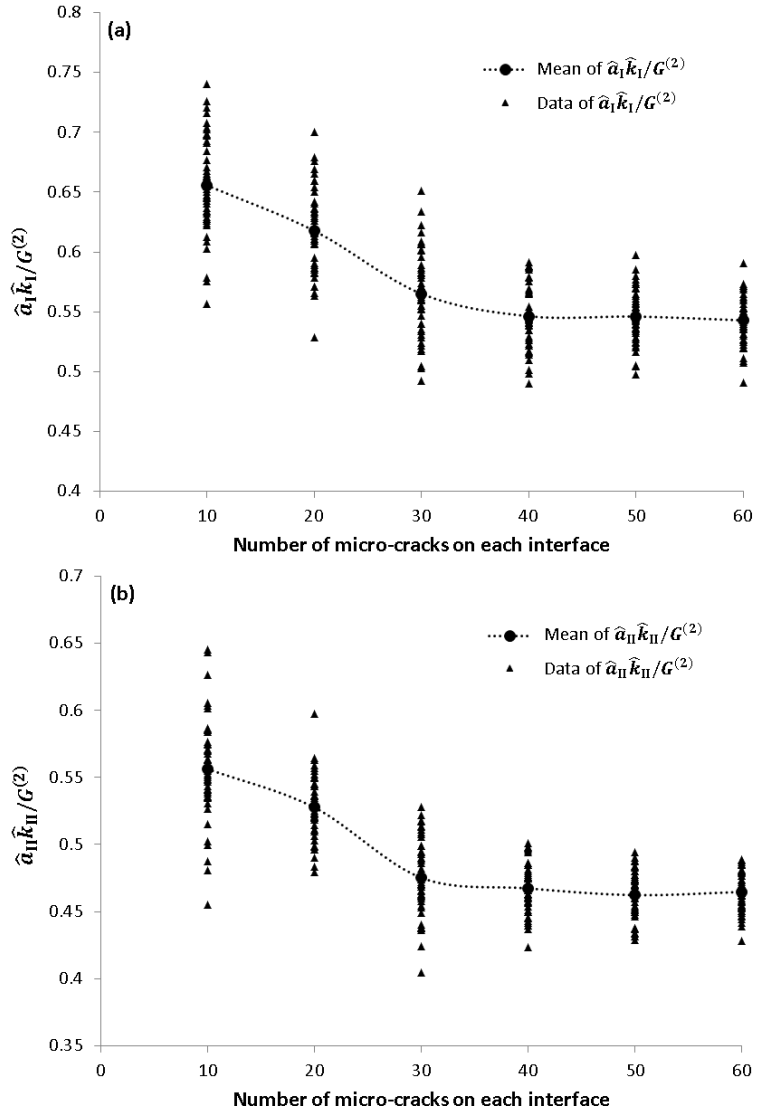

Figure 4. Scatter plots and mean values of $\widehat{a}_{\mathrm{I}}\widehat{k}_{\mathrm{I}}/G^{(2)}$ and $\widehat{a}_{\mathrm{II}}\widehat{k}_{\mathrm{II}}/G^{(2)}$ against M for $\rho_{\mathrm{I}} = 0.7$, $\rho_{\mathrm{II}} = 0.5$, $\widehat{a}_{\mathrm{I}}/h = 1$, $G^{(1)}/G^{(2)} = 0.5$ and $G^{(3)}/G^{(2)} = 2$.

5.2 Effect of the micro-crack length distribution

The effect of the micro-crack length distribution on the mean values of the non-dimensionalized effective stiffness $\widehat{a}_{\rm I}\widehat{k}_{\rm I}/G^{(2)}$ and $\widehat{a}_{\rm II}\widehat{k}_{\rm II}/G^{(2)}$ is examined here. For fixed values of $\rho_{\rm I}$, $\rho_{\rm II}$, $\widehat{a}_{\rm I}/h$, $G^{(1)}/G^{(2)}$ and $G^{(3)}/G^{(2)}$, a sample of 50 pairs of randomly generated interfaces is used for estimating the effective stiffness $\widehat{a}_{\rm I}\widehat{k}_{\rm I}/G^{(2)}$ and $\widehat{a}_{\rm II}\widehat{k}_{\rm II}/G^{(2)}$. As suggested in Subsection 5.1, the number of the micro-cracks over a period interval of each interface is taken to be 40. For both interfaces I and II, the micro-crack lengths follow a $\chi^2(k)$ distribution.

To investigate how the different values of the degree of freedom k (that is, different micro-crack length distributions) affect the effective stiffness for both interfaces I and II, we plot the mean values of $\widehat{a}_{\rm I}\widehat{k}_{\rm I}/G^{(2)}$ against $\rho_{\rm I}$ for cases where the micro-cracks along both interfaces I and II are generated by the $\chi^2(5)$, $\chi^2(10)$ and $\chi^2(25)$ distributions for $\rho_{\rm I} = \rho_{\rm II}$, $G^{(1)}/G^{(2)} = G^{(3)}/G^{(2)} = 10$ and $\widehat{a}_{\rm I}/h = 2$ in Figure 5. Values of $\widehat{a}_{\rm I}\widehat{k}_{\rm I}/G^{(2)}$ predicted by the three-phase model in Subsection 4.2 are also plotted against $\rho_{\rm I}$ in Figure 5. Note that here values of $\widehat{a}_{\rm II}\widehat{k}_{\rm II}/G^{(2)}$ are very close to $\widehat{a}_{\rm I}\widehat{k}_{\rm I}/G^{(2)}$.

It is obvious that the non-dimensionalized effective stiffness $\widehat{a}_{\rm I}\widehat{k}_{\rm I}/G^{(2)}$ becomes closer to the corresponding value predicted by the three-phase model as the degree of freedom k of the χ^2 distribution increases, that is, as the micro-crack lengths generated by the χ^2 distributions become more normal-like. This may be explained as follows. The ratio of the standard deviation of the χ^2 distribution to the mean of the distribution is given by $\sqrt{2/k}$. This ratio tends to zero as k increases. Thus the micro-cracks generated by the χ^2 distribution with a very large k may be regarded to be of equal length and evenly distributed on each of the two interfaces. Note that the three-phase model assumes that the micro-cracks on each interface are of equal length

and evenly distributed on the interface.

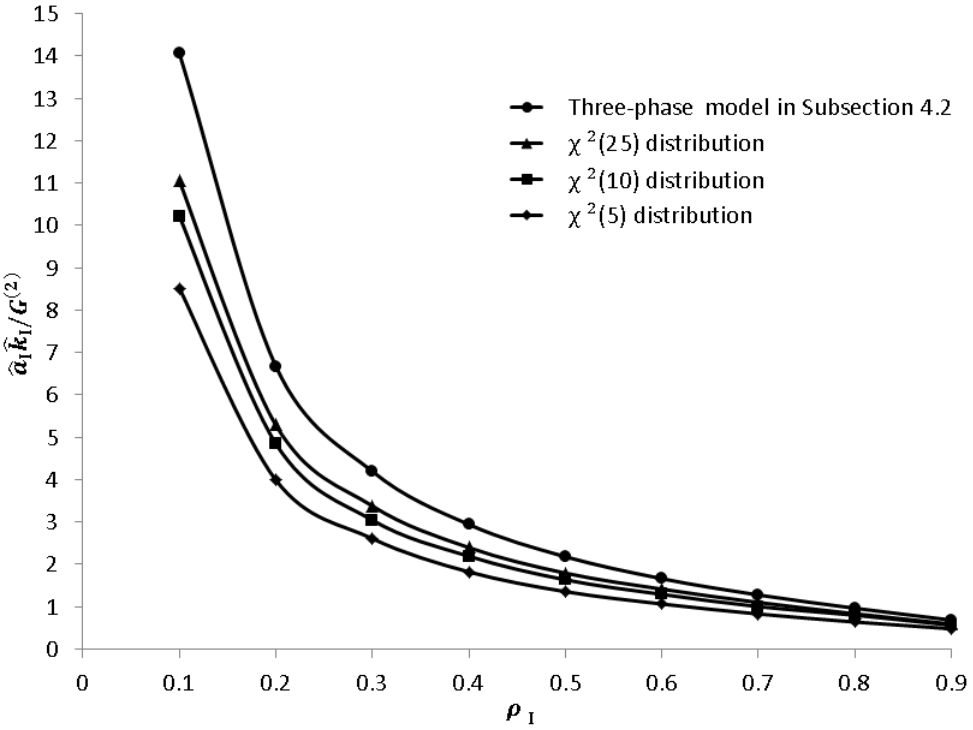

Figure 5. Plots of $\widehat{a}_{\rm I}\widehat{k}_{\rm I}/G^{(2)}$ against $\rho_{\rm I}$ for cases where the micro-cracks along both interfaces I and II are generated by the $\chi^2(5)$, $\chi^2(10)$ and $\chi^2(25)$ distributions for $\rho_{\rm I} = \rho_{\rm II}$, $G^{(1)}/G^{(2)} = G^{(3)}/G^{(2)} = 10$ and $\widehat{a}_{\rm I}/h = 2$. Also included are the plots of the corresponding effective stiffness predicted by the three-phase model.

5.3 Effects of the elastic moduli, the thickness of the layer and the damage ratios

The effects of the elastic moduli, the thickness of the layer and the damage ratios on the effective stiffness coefficients $\widehat{k}_{\rm I}$ and $\widehat{k}_{\rm II}$ are examined here. As before, for fixed values of $\rho_{\rm I}$, $\rho_{\rm II}$, $\widehat{a}_{\rm I}/h$, $G^{(1)}/G^{(2)}$ and $G^{(3)}/G^{(2)}$, 50 pairs of

interfaces are randomly generated for the statistical simulations. For each pair of interfaces, the number of the micro-cracks over a period interval of each interface is taken to be 40. For each interface, the lengths of the micro-cracks are randomly generated by using the $\chi^2(5)$ distribution.

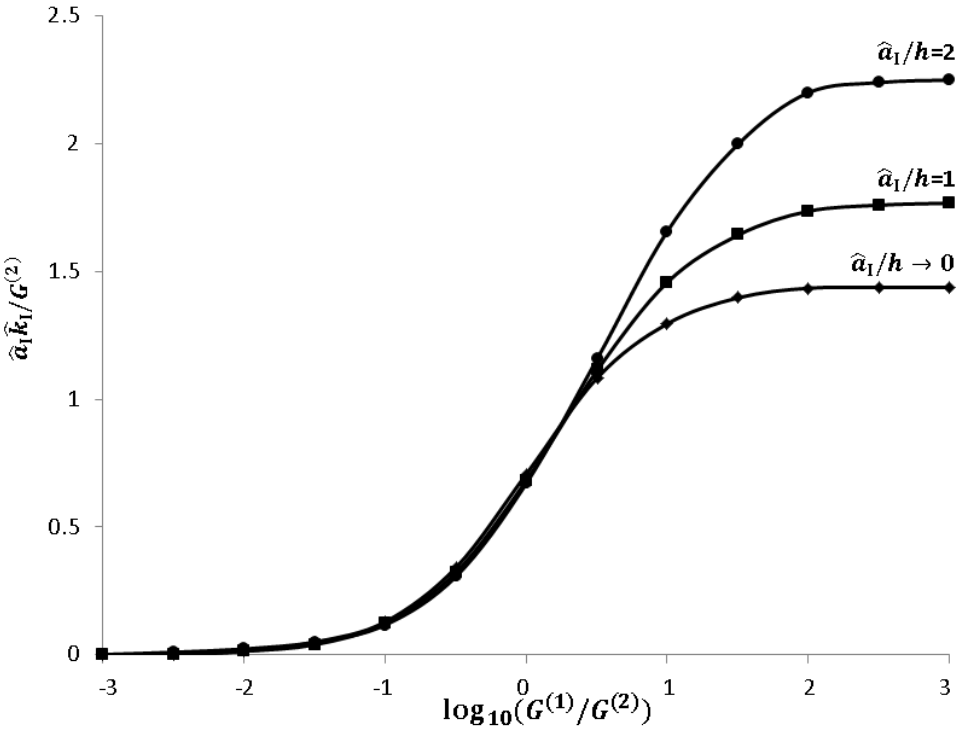

Figure 6. Plots of $\widehat{a}_{\rm I}\widehat{k}_{\rm I}/G^{(2)}$ against $\log_{10}(G^{(1)}/G^{(2)})$ for $\rho_{\rm I} = \rho_{\rm II} = 0.5$, $G^{(1)}/G^{(2)} = G^{(3)}/G^{(2)}$ and selected values of $\widehat{a}_{\rm I}/h$.

For $\rho_{\rm I} = \rho_{\rm II} = 0.5$ and $G^{(1)}/G^{(2)} = G^{(3)}/G^{(2)}$, Figure 6 plots the non-dimensionalized effective stiffness $\widehat{a}_{\rm I}\widehat{k}_{\rm I}/G^{(2)}$ against $\log_{10}(G^{(1)}/G^{(2)})$ for selected values of $\widehat{a}_{\rm I}/h$. As expected, the values of $\widehat{a}_{\rm II}\widehat{k}_{\rm II}/G^{(2)}$ are observed to be very close to $\widehat{a}_{\rm I}\widehat{k}_{\rm I}/G^{(2)}$. For larger values of $G^{(1)}/G^{(2)}$ within the range $0.5 \leq \log_{10}(G^{(1)}/G^{(2)}) \leq 3$, the plots of the non-dimensionalized effective

stiffness for the different values of $\widehat{a}_{\rm I}/h$ are visually distinguishable. For a selected $G^{(1)}/G^{(2)}$ such that $0.5 \leq \log_{10}(G^{(1)}/G^{(2)}) \leq 3$, the value of $\widehat{a}_{\rm I}\widehat{k}_{\rm I}/G^{(2)}$ is larger for larger $\widehat{a}_{\rm I}/h$. For $G^{(1)}/G^{(2)} > 100$, $\widehat{a}_{\rm I}\widehat{k}_{\rm I}/G^{(2)}$ increases very slowly with increasing $G^{(1)}/G^{(2)}$. For a fixed value of $\widehat{a}_{\rm I}/h$, it appears that $\widehat{a}_{\rm I}\widehat{k}_{\rm I}/G^{(2)}$ tends to a constant as $G^{(1)}/G^{(2)}$ increases. The thickness of the thin layer seems to have an obvious effect on the effective stiffness only if the elastic material for the thin layer is soft enough compared to the materials in the two half-spaces. As $G^{(1)}/G^{(2)} \to 0^+$, the values of $\widehat{a}_{\rm I}\widehat{k}_{\rm I}/G^{(2)}$ tend to zero, that is, if the thin layer is extremely hard relative to the two half-spaces, the magnitudes of the effective stiffness for both interfaces I and II may be very small.

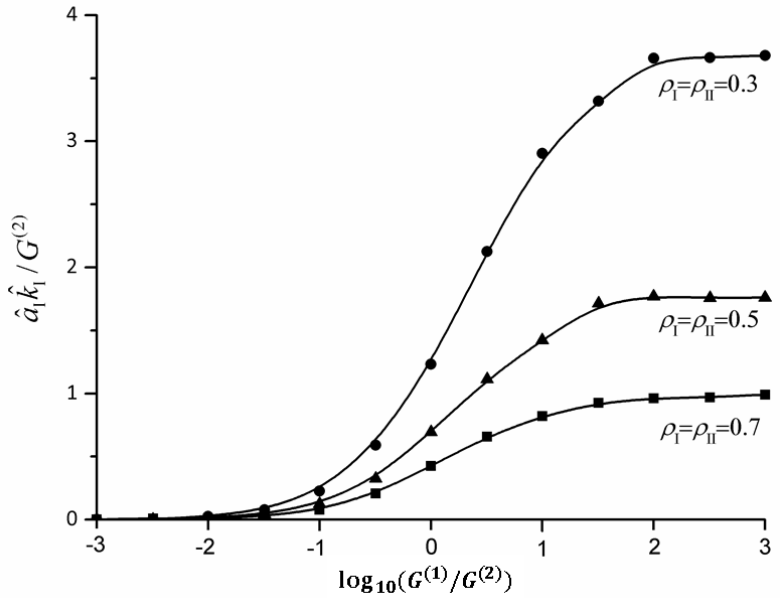

Figure 7. Plots of $\widehat{a}_{\rm I}\widehat{k}_{\rm I}/G^{(2)}$ against $\log_{10}(G^{(1)}/G^{(2)})$ for $\widehat{a}_{\rm I}/h = 1$, $G^{(1)}/G^{(2)} = G^{(3)}/G^{(2)}$, $\rho_{\rm I} = \rho_{\rm II} = 0.3$, 0.5 and 0.7.

In Figure 7, $\widehat{a}_{\rm I}\widehat{k}_{\rm I}/G^{(2)}$ is plotted against $\log_{10}(G^{(1)}/G^{(2)})$ for $\widehat{a}_{\rm I}/h = 1$, $G^{(1)}/G^{(2)} = G^{(3)}/G^{(2)}$, $\rho_{\rm I} = \rho_{\rm II} = 0.3$, 0.5 and 0.7. Values of $\widehat{a}_{\rm II}\widehat{k}_{\rm II}/G^{(2)}$ are very close to $\widehat{a}_{\rm I}\widehat{k}_{\rm I}/G^{(2)}$. It is observed that the non-dimensionalized effective stiffness $\widehat{a}_{\rm I}\widehat{k}_{\rm I}/G^{(2)}$ is larger when the two interfaces have smaller damage ratios. This is not surprising as the micro-cracks are more stable and hence the displacement jumps over the micro-cracks are smaller when the micro-cracks are less densely located on the interface.

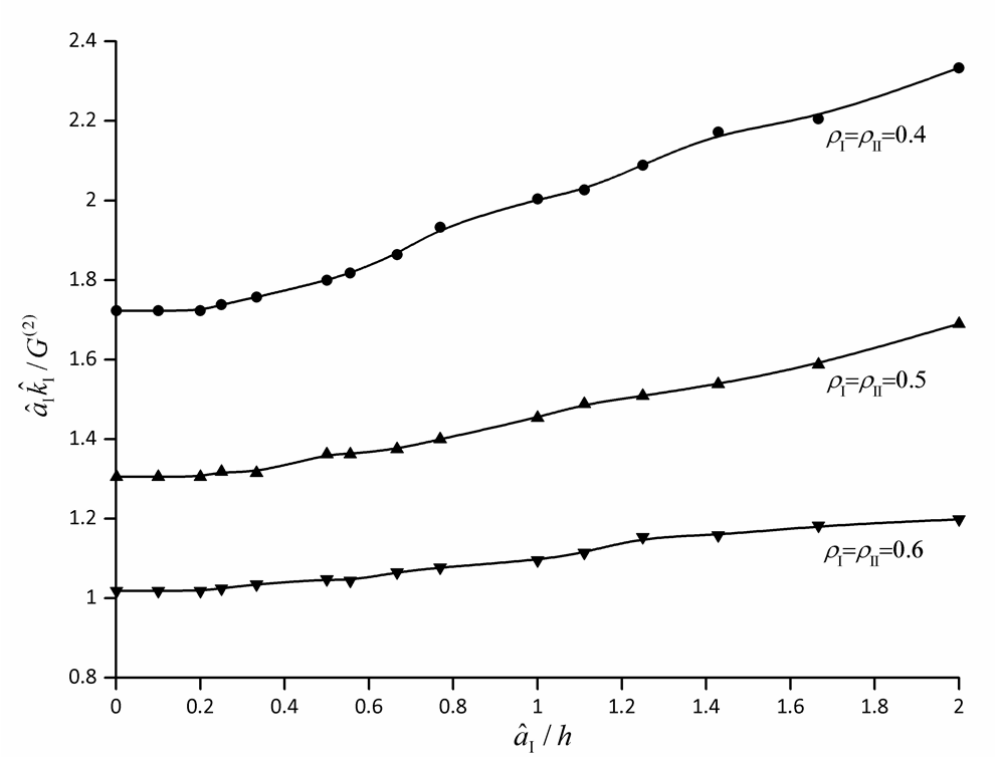

Figure 8. Plots of $\widehat{a}_{\rm I}\widehat{k}_{\rm I}/G^{(2)}$ against $\widehat{a}_{\rm I}/h$ for $G^{(1)}/G^{(2)} = G^{(3)}/G^{(2)} = 10$, $\rho_{\rm I} = \rho_{\rm II} = 0.4$, 0.5 and 0.6.

For relatively large values of $G^{(1)}/G^{(2)}$ and $G^{(3)}/G^{(2)}$ given by $G^{(1)}/G^{(2)} = G^{(3)}/G^{(2)} = 10$, the non-dimensionalized effective stiffness $\widehat{a}_{\rm I}\widehat{k}_{\rm I}/G^{(2)}$ is plotted

against $\widehat{a}_{\rm I}/h$ in Figure 8 for $\rho_{\rm I} = \rho_{\rm II} = 0.4$, 0.5 and 0.6. For a fixed value of $\rho_{\rm I}$, the effective stiffness increases as $\widehat{a}_{\rm I}/h$ increases. This is as expected, as the micro-cracks on the parallel planes $x_2 = 0$ and $x_2 = h$ are more stable having smaller displacement jumps over the micro-cracks when the distance between the planes are smaller. The statistical simulations for other values of $\rho_{\rm I} = \rho_{\rm II}$ and $G^{(1)}/G^{(2)} = G^{(3)}/G^{(2)}$ within the range $0.1 \le \rho_{\rm I} \le 0.9$ and $0.5 \le \log_{10}(G^{(1)}/G^{(2)}) \le 3$ give the similar results.

Figure 8 also shows that the values of $a_{\rm I}\widehat{k}_{\rm I}/G^{(2)}$ tend to the corresponding effective stiffness calculated in Wang *et al.* [17] as $a_{\rm I}/h \to 0^+$ for a fixed $\rho_{\rm I}$. In [17], a micro-cracked interface between two dissimilar elastic half-spaces under antiplane deformations is formulated to calculate the effective stiffness of the damaged interface. Note that as $a_{\rm I}/h$ tends to 0^+ here each of the micro-cracked interfaces in Figure 1 may be regarded as an interface between two dissimilar elastic half-spaces.

For $\rho_{\rm I} = 0.5$ and $G^{(1)}/G^{(2)} = G^{(3)}/G^{(2)} = 10$, Figure 9 plots the non-dimensionalized effective stiffness coefficients $\widehat{a}_{\rm I}\widehat{k}_{\rm I}/G^{(2)}$ and $\widehat{a}_{\rm II}\widehat{k}_{\rm II}/G^{(2)}$ against $\rho_{\rm II}$ for selected values of $\widehat{a}_{\rm I}/h$. For a fixed value of $\widehat{a}_{\rm I}/h$, both $\widehat{a}_{\rm I}\widehat{k}_{\rm I}/G^{(2)}$ and $\widehat{a}_{\rm II}\widehat{k}_{\rm II}/G^{(2)}$ become smaller as $\rho_{\rm II}$ increases, as may be expected. This observation is not surprising as increasing the damage ratio on the interface II has the effect of increasing the displacement jumps over the micro-cracks on both interfaces I and II. Note that for a fixed $\widehat{a}_{\rm I}/h$ the effective stiffness coefficient $\widehat{a}_{\rm I}\widehat{k}_{\rm I}/G^{(2)}$ tends to a certain finite value but $a_{\rm II}\widehat{k}_{\rm II}/G^{(2)}$ tends to infinity as $\rho_{\rm II}$ approaches zero, that is, as interface II becomes more perfectly bonded like. For a fixed $\widehat{a}_{\rm I}/h$, $\widehat{a}_{\rm II}\widehat{k}_{\rm II}/G^{(2)}$ decreases more drastically than $\widehat{a}_{\rm I}\widehat{k}_{\rm I}/G^{(2)}$ as $\rho_{\rm II}$ increases from 0.05 to 0.9. Calculations using other values of $\rho_{\rm I}$, $\widehat{a}_{\rm I}/h$ and $G^{(1)}/G^{(2)} = G^{(3)}/G^{(2)}$ within the ranges $0.05 \le \rho_{\rm I} \le 0.9$, $0 < \widehat{a}_{\rm I}/h \le 2$ and $0.001 \le G^{(1)}/G^{(2)} \le 1000$ show similar observations.

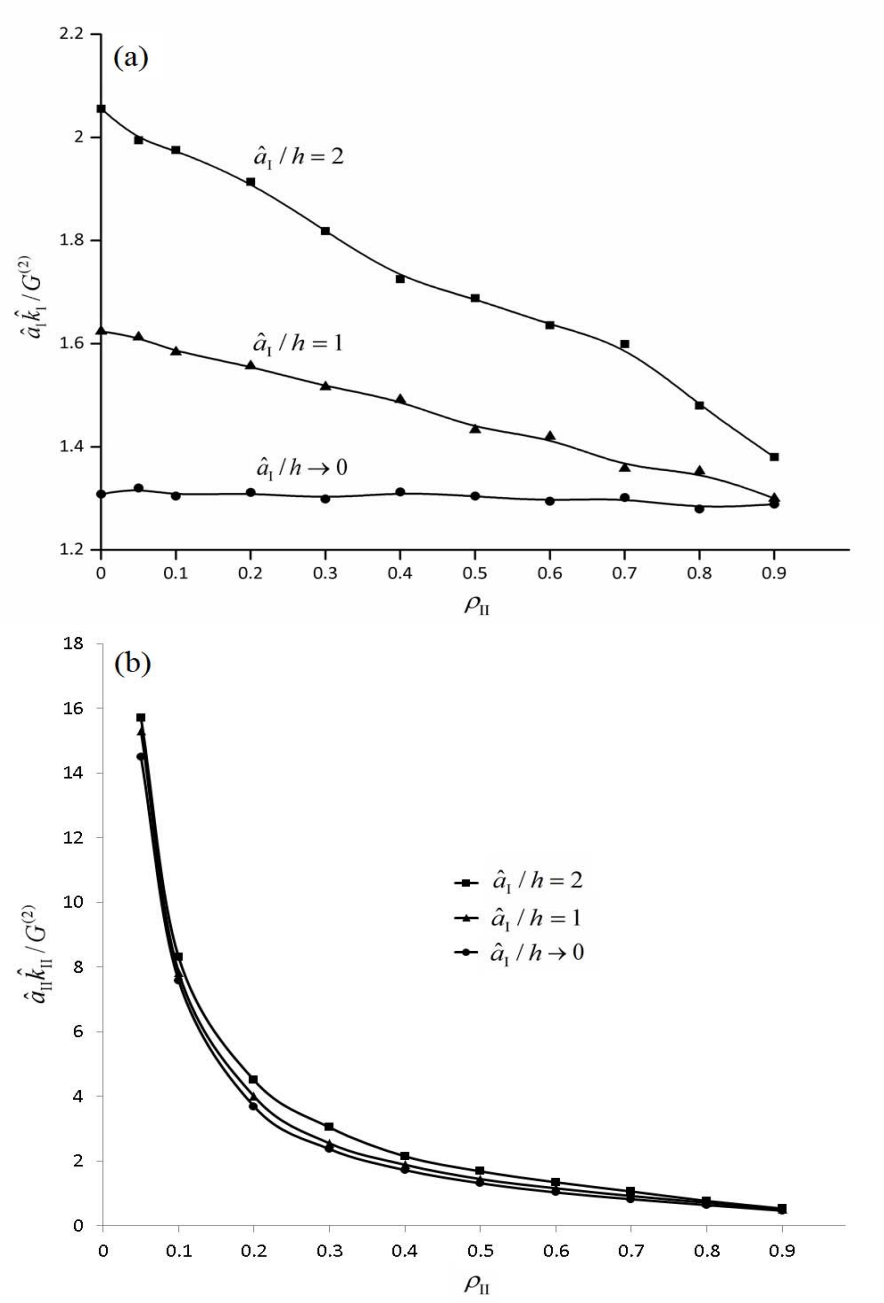

Figure 9. Plots of $\widehat{a}_{\mathrm{I}}\widehat{k}_{\mathrm{I}}/G^{(2)}$ and $\widehat{a}_{\mathrm{II}}\widehat{k}_{\mathrm{II}}/G^{(2)}$ against ρ_{II} for $\rho_{\mathrm{I}} = 0.5$, $G^{(1)}/G^{(2)} = G^{(3)}/G^{(2)} = 10$ and selected values of $\widehat{a}_{\mathrm{I}}/h$.

6 Summary

A micromechanical-statistical model is proposed in the present paper for the purpose of estimating the effective stiffness coefficients of a pair of microscopically damaged interfaces in a trimaterial under antiplane deformations. The trimaterial is made of an thin elastic layer sandwiched between two elastic half-spaces — the two microscopically damaged interfaces are parallel planes. The interfaces are modeled as containing periodic arrays of micro-cracks. On each interface, an arbitrary number of micro-cracks whose lengths follow a chosen chi-square distribution (χ^2) are randomly positioned on a period interval of the interface. The micromechanical-statistical model is formulated and numerically solved in terms of hypersingular integral equations.

The hypersingular integral formulations for the micromechanical-statistical model are verified by comparing the values of the effective stiffness coefficients computed for the special case where each of the interfaces has evenly distributed micro-cracks of equal length with the corresponding values calculated by a three-phase model. The two sets of values show good agreement for wide ranges of parameters.

For the micromechanical-statistical model, the simulations carried out here suggest that at least 40 micro-cracks on each interface are required to homogenize the effective stiffness of the interface. Cases where the micro-crack lengths for the two interfaces are generated by the χ^2 distribution of a higher degree of freedom give effective stiffness coefficients closer to the ones predicted by the three-phase model.

The micromechanical-statistical model is used to study the effects of the elastic moduli, the thickness of the layer and the damage ratios on the effec-

tive stiffness coefficients. We observe that the effect of varying the thickness of the thin layer on the effective stiffness coefficients is only obvious when the thin layer is sufficiently soft compared to the two half-spaces. If the thin layer is soft enough relative to the two half-spaces, the effective stiffness coefficients increase as the thickness of the thin layer decreases. For fixed elastic moduli of the trimaterial and a fixed non-dimensionalized thin layer thickness, the effective stiffness coefficients decrease as the damage ratios of the two interfaces increase.

References

[1] M. Abramowitz and I. Stegun, *Handbook of Mathematical Functions*, Dover, New York, 1970.

[2] W. T. Ang, Elastodynamic antiplane deformation of a bimaterial with an imperfect viscoelastic interface: a dual reciprocity hypersingular boundary integral solution, *Applied Mathematical Modelling* **31** (2007) 749-769.

[3] W. T. Ang, *Hypersingular Integral Equations in Fracture Analysis,* Woodhead Publishing, Cambridge, 2013.

[4] Y. Benveniste and T. Miloh, Imperfect soft and stiff interfaces in two-dimensional elasticity, *Mechanics of Materials* **33** (2001) 309-323.

[5] J. R. Berger and V. K. Tewary, Green's functions for boundary element analysis of anisotropic bimaterials, *Engineering Analysis with Boundary Elements* **25** (2001) 279-288.

[6] R. M. Christensen and K. H. Lo, Solutions for effective shear properties in three phase sphere and cylinder models, *Journal of the Mechanics and Physics of Solids* **27** (1979) 315-330.

[7] D. L. Clements, *Boundary Value Problems Governed by Second Order Elliptic Systems*, Pitman, London, 1981.

[8] H. Fan and K. Y. Sze, A micro-mechanics model for imperfect interface in dielectric materials, *Mechanics of Materials* **33** (2001) 363-370.

[9] H. Fan and G. F. Wang, Interaction between a screw dislocation and viscoelastic interfaces, *International Journal of Solids and Structures* **40** (2003) 763-776.

[10] Z. Hashin, The spherical inclusion with imperfect interface, *ASME Journal of Applied Mechanics* **58** (1991) 444-449.

[11] J. P. Jones and J. S. Whittier, Waves at a flexibly bonded interface, *Journal of Applied Mechanics* **34** (1967) 905-909.

[12] A. C. Kaya and F. Erdogan, On the solution of integral equations with strongly singular kernels, *Quarterly of Applied Mathematics* **45** (1987) 105-122.

[13] W. Knoll and R. C. Advincula, *Functional Polymer Films*, Wiley-VCH, Weinheim, 2011.

[14] F. París and J. Cañas, *Boundary Element Method: Fundamentals and Applications*, Oxford University Press, Oxford, 1997.

[15] W. H. Press, S. A. Teukolsky, W. T. Vetterling and B. P. Flannery, *Numerical Recipes: The Art of Scientific Computing*, Cambridge University Press, Cambridge, 2007.

[16] X. Wang, W. T. Ang and H. Fan, Micro-mechanics models for an imperfect interface under anti-plane shear load: Hypersingular integral formulations, *Engineering Analysis with Boundary Elements* **36** (2012) 1856-1864.

[17] X. Wang, H. Fan and W. T. Ang, On micromechanical-statistical modeling of microscopically damaged interfaces under antiplane deformations, *International Journal of Solids and Structures* **51** (2014) 2327-2335.

[18] X. C. Zhang, B. S. Xu, H. D. Wang and Y. X. Wu, An analytical model for predicting thermal residual stresses in multilayer coating systems, *Thin Solid Films* **488** (2005) 274-282.